Phase-amplitude reduction far beyond the weakly perturbed paradigm

Dan Wilson

Phys. Rev. E **101**, 022220 — Published 25 February 2020

DOI: 10.1103/PhysRevE.101.022220

Phase-Amplitude Reduction Far Beyond the Weakly Perturbed Paradigm

Dan Wilson[1]

[1]Department of Electrical Engineering and Computer Science, University of Tennessee, Knoxville, TN 37996, USA

January 27, 2020

Abstract

While phase reduction is a well-established technique for the analysis of perturbed limit cycle oscillators, practical application requires perturbations to be sufficiently weak thereby limiting its utility in many situations. Here, a general strategy is developed for constructing a set of phase-amplitude reduced equations that is valid to arbitrary orders of accuracy in the amplitude coordinates. This reduction framework can be used to investigate the behavior of oscillatory dynamical systems far beyond the weakly perturbed paradigm. Additionally, a patchwork phase-amplitude reduction method is suggested that is useful when exceedingly large magnitude perturbations are considered. This patchwork method incorporates the high-accuracy phase-amplitude reductions of multiple nearby periodic orbits that result from modifications to nominal parameters. The proposed method of high-accuracy phase-amplitude reduction can be readily implemented numerically and examples are provided where reductions are computed up to fourteenth order accuracy.

1 Introduction

Many physical, chemical, and biological systems exhibit stable oscillations. Over the proceeding decades, phase reduction has become an essential tool [1], [2], [3], [4], [5], [6], [7]. for analyzing and understanding these oscillatory behaviors in complicated and high-dimensional dynamical systems. This strategy can be used to represent the state of an N-dimensional oscillatory system in terms of a single phase variable that gives a sense of the timing of the oscillation. Phase reduction has facilitated the discovery of fundamental mechanisms that govern complex patterns emerging in populations of both weakly forced and weakly interacting oscillators [8], [9], [10], [11], [12].

While phase reduction is a tremendously powerful tool, it requires the dynamical system under study to remain close to its unperturbed periodic orbit. As the magnitude of perturbations increase, the applicability of the phase reduction begins to degrade often leading to inaccurate predictions about the dynamical behavior. Recent years have seen a sustained interest in the development of phase reduction techniques that can be used to understand oscillatory dynamical behavior beyond the weakly perturbed paradigm. For instance, [13] and [14] investigate phase reduced frameworks applicable to strongly perturbed oscillators provided the applied perturbation varies slowly. A related strategy [15] investigates strongly perturbed oscillators in response to high-frequency forcing. Others have focused on frameworks that can compute the phase coordinates (i.e., isochrons) in the fully nonlinear basin of attraction of the limit cycle [16], [17], a strategy that only proves useful in

low-dimensional settings because it does not yield a reduction in dimensionality. Koopman operator based strategies have shown promise [18], however, it is not usually readily apparent how to find a suitable basis to represent the system observables. Others have investigated alternative definitions of phase that correspond to some important feature of the underlying dynamical system. The notions of local orthogonal rectification [19], entrainment maps [20], operational phase coordinates [21], functional phase response curves [22], and stochastic phase [23] result from using different characterizations of phase; each has its own benefits and drawbacks, but none are particularly well suited for studying system response to strong perturbations.

In this work, the notion of isostable coordinates will be used to develop a general phase-amplitude reduction framework valid to arbitrary orders of accuracy. As compared to standard phase reduction methods, increasing the order of accuracy can make the resulting phase reduced equations more applicable when considering large amplitude inputs. As part of the proposed reduction strategy, isostable coordinates will be used to characterize the transient behavior of solutions in directions transverse to the periodic orbit. The notion of isostable coordinates was first suggested for dynamical systems with stable fixed points in the context of level sets of the slowest decaying Koopman eigenfunction [24]; the notion of isostables was subsequently adapted for periodic orbits [25], [26], [27]. A defining feature of isostable coordinates is that they have an exponential decay within the basin of attraction of the limit cycle governed by the Floquet exponents associated with the local linearization about the limit cycle. In most high-dimensional systems, many isostable coordinates decay rapidly allowing them to be effectively ignored resulting in a significant decrease in dimensionality compared to the original equation [5]. This phase-amplitude reduction framework has been used previously to develop general reduction frameworks that provide second order corrections to the standard phase reduced equations [28], [29], but no general strategy currently exists for computing reductions that are valid to higher orders of accuracy. Related strategies have been developed recently to compute phase reduced equations that are valid to second and third order in the perturbation strength [30], [31], but these remain difficult to implement for higher orders of accuracy in general models. The strategy presented in this work can readily be implemented in dynamical systems with arbitrarily high dimension; examples to follow compute phase-amplitude reductions that are valid to fourteenth order accuracy in the amplitude coordinates.

The organization of this paper is as follows: Section 2 provides necessary background on the notions of phase, isochrons, and isostable coordinates as used for phase-amplitude reduction. Section 3 gives a general strategy for implementing phase-amplitude reduction to arbitrary orders of accuracy in the isostable coordinates. Section 4 illustrates a strategy that can be effective when working with particularly large perturbations—a so-called patchwork phase-amplitude reduction strategy is suggested whereby a high-accuracy phase-amplitude reduction is computed for multiple nearby orbits and the the nominal reduced dynamics seamlessly switch between them. Section 5 provides two illustrative examples highlighting the utility of this reduction framework and Section 6 gives concluding remarks.

2 Background on Phase-Amplitude Reduction Using Isostable Coordinates

Consider a general ordinary differential equation of the form

$$\dot{x} = F(x) + U(t), \tag{1}$$

where $x \in \mathbb{R}^N$ is the state, F represents the underlying dynamics, and $U(t)$ represents a time-dependent perturbation. Suppose that when $U(t) = 0$ (i.e., in the absence of perturbation) Equation

(1) has a stable T-periodic orbit denoted by $x^\gamma(t)$. In applications where timing of oscillatory behavior is of interest (e.g., synchronization, entrainment, etc.), the notion of phase is often used to work with (1) in a reduced setting. To do so, for the moment taking $U(t) = 0$, all locations on the periodic orbit can be assigned a phase $\theta \in [0, 2\pi)$ scaled so that $d\theta/dt = \omega$ with $\omega = 2\pi/T$. Using the concept of isochrons [1], [32], the notion of phase can be extended to the basin of attraction of the limit cycle $\mathcal{B}^\gamma$, i.e., the set of all initial conditions that approach the limit cycle as time approaches infinity. In this manner, letting θ_1 be the phase corresponding to $a(0) \in x^\gamma$, the θ_1 isochron (i.e., level set of phase θ_1) can be defined as the set of all $b(0) \in \mathcal{B}^\gamma$ such that

$$\lim_{t\to\infty} ||a(t) - b(t)|| = 0, \tag{2}$$

where $||\cdot||$ can be any norm. By extending phase to the basin of attraction of the limit cycle using isochrons, one can show that when $U(t) = 0$, the associated phase for any trajectory $x(t)$ of (1) evolves in time according to $d\theta/dt = \omega$. Intuitively, Equation (2) encodes for the infinite time convergence to the 1-dimensional periodic orbit. The notion of isochrons can be used to perform a phase reduction that views the nominal system in terms of the timing of its oscillations rather than the underlying state. From this perspective, one can transform (1) to a system of the form

$$\dot{\theta} = \omega + Z(\theta) \cdot U(t), \tag{3}$$

where $Z(\theta)$ is a phase response curve that represents the gradient of the phase coordinates evaluated at $x^\gamma(\theta)$, and "$\cdot$" denotes the dot product. In the preceding decades, phase reduction has been applied extensively to illuminate the mechanisms driving complicated behaviors observed in weakly perturbed oscillatory dynamical systems, [1], [6], [3], [4], [2].

While phase reduction is a widely used strategy for studying weakly perturbed oscillators, its assumptions break down as the magnitude of $U(t)$ becomes larger and the state is driven farther from the underlying limit cycle. In order to remedy this and increase the accuracy of the phase dynamics for larger perturbations, additional information about the transient dynamics transverse to the limit cycle, often referred to as amplitude coordinates, must be included. Many coordinate frameworks have been developed to characterize the behavior of amplitude coordinates [33], [23], [34], [35], [27], [26]. This work will use an isostable coordinate framework, which gives a sense of the infinite time decay of perturbations transverse to the limit cycle [26] (cf., [27],[35]). To a linear approximation, an isostable coordinate transformation can be identified using Floquet theory [36]. To do so, let $\Delta x = x(\theta) - x^\gamma(\theta)$ denote the difference between some state and another state on the periodic orbit with identical phase. To a linear approximation, one can write

$$\Delta\dot{x} = J\Delta x, \tag{4}$$

where J denotes the Jacobian evaluated at $x^\gamma(\theta)$. Note that the Jacobian from (4) is time varying. Let Φ denote a fundamental matrix such that $x(T) = \Phi x(0)$ for initial solutions of $x(0)$ with phase θ. Provided Φ is diagonalizable, to a linear approximation solutions near the periodic orbit can be characterized according to

$$x(\theta, \psi_1, \ldots, \psi_{N-1}) = x^\gamma(\theta) + \sum_{k=1}^{N-1} \psi_k g^k(\theta) + \mathcal{O}(\psi_1^2) + \cdots + \mathcal{O}(\psi_{N-1}^2), \tag{5}$$

where $g^k(\theta)$ is a Floquet eigenfunction of (4), and ψ_k is an isostable coordinate with unperturbed dynamics that follow $\dot{\psi}_k = \kappa_k\psi_k$ with κ_k being a Floquet multiplier. Notice that in (5), the isostable coordinates give a sense of the distance from the periodic orbit. The characteristic feature

of isostable coordinates is that they decay at a constant exponential rate in the absence of input. While Floquet theory can be used to define $N-1$ isostable coordinates in a neighborhood of the periodic orbit, for some of the smallest magnitude Floquet exponents, it is possible to explicitly define isostable coordinates in the entire basin of attraction of the limit cycle using the infinite time relaxation to the periodic orbit. Letting $\lambda_j = \exp(\kappa_j T)$ be an eigenvalue of the fundamental matrix, Φ, with an associated left eigenvector w_j, the slowest decaying isostable coordinates can be explicitly defined according to [26]:

$$\psi_j(x) = \lim_{k\to\infty} \left[w_j^T (\nu(t_\Gamma^k, x) - x_0) \exp(-\kappa_j t_\Gamma^k) \right], \tag{6}$$

where t_Γ^k denotes the time of the k^{th} transversal of the Γ_0 isochron and $\nu(t,x)$ is the unperturbed flow of (1). Equation (6) is defined in relation to the infinite time relaxation to the periodic orbit. Intuitively, as k approaches infinity, the growth rate of the term $\exp(-\kappa_k t_\Gamma^k)$ matches the decay rate of $w_j^T(\nu(t_\Gamma^k, x) - x_0)$ so that (6) converges to the isostable coordinate.

For rapidly decaying isostable coordinates, there is no constructive definition like (6). Rather, isostable coordinates ψ_j associated with larger magnitude κ_j can be thought of as level sets of Koopman eigenfunctions with decay rates that are governed by the Floquet exponents of the linearized system. For a more detailed treatment of expansions of dynamical systems in terms of Koopman eigenfunctions, the interested reader is referred to [37], [38]. Intuitively, isostables as considered in this work can be thought of as amplitude coordinates of the periodic orbit that decay according to $\dot{\psi}_j = \kappa_j \psi_j$ in the absence of external perturbation.

While isochrons and isostables can be defined in the fully nonlinear basin of attraction of the limit cycle, they can be difficult to work with directly because they require knowledge of θ and ψ_j as functions of x. Additionally, direct computation of phase and isostable coordinates is challenging for high-dimensional systems as the direct consequence of Bellman's 'curse of dimensionality'; practical examples computing isochrons directly have been limited to $N = 4$ dimensions [17], [35], [39]. For this reason, closed form asymptotic expansions near the periodic orbit (which are the primary focus of this work) are usually more useful. Previous work [28], [29], [26] has investigated closed-form, reduced order equations that characterize the perturbed dynamics of the phase and isostable coordinates according to:

$$\begin{aligned}
\dot{\theta} &= \omega + \left(Z(\theta) + \sum_{k=1}^{M} \psi_k B^k(\theta) \right) \cdot U(t), \\
\dot{\psi}_j &= \kappa_j \psi_j + \left(I_j(\theta) + \sum_{k=1}^{M} \psi_k C_j^k(\theta) \right) \cdot U(t), \\
j &= 1, \ldots, M,
\end{aligned} \tag{7}$$

where and $M < N-1$. Here, $Z(\theta)$ and $I_j(\theta)$ are often referred to as phase and isostable response curves, respectively, and represent the gradient of the phase and isostable coordinates evaluated on the periodic orbit at phase θ. Computation of these functions is usually accomplished identifying adjoint eigenfunctions of (4) [40], [25], [41], and are the appropriately normalized periodic solutions to

$$\begin{aligned}
\left.\frac{dZ}{dt}\right|_\theta &= -J^T Z(\theta), \\
\left.\frac{dI_k}{dt}\right|_\theta &= (\kappa_k \mathrm{Id} - J^T) I_k(\theta),
\end{aligned} \tag{8}$$

where ^{T} denotes the matrix transpose and Id is an appropriately sized identity matrix. The functions $B^k(\theta)$ and $C^k_j(\theta)$ provide second order corrections to the dynamics as the state is perturbed from the periodic orbit, and have been used to identify bifurcations resulting from nonlinear interactions due to coupling [42] and to investigate how phase response depends on prior perturbations [29]. Strategies for computation of $B^k(\theta)$ and $C^k_j(\theta)$ are discussed in detail in [28]. Many dynamical systems have Floquet exponents that are negative and large in magnitude. In practice, it is often possible to define some threshold $\kappa_{\text{thresh}} > 0$ and ignore any isostable coordinates ψ_k with corresponding Floquet exponent $|\kappa_k| > \kappa_{\text{thresh}}$ since perturbations to those coordinates decay rapidly yielding $M < N-1$ isostable coordinates that must be accounted for in the reduction (7).

3 Phase and Isostable Reduction with Arbitrary Accuracy

While isostable coordinates provide a useful framework from which to investigate the perturbed behavior of high-dimensional dynamical systems, it still has many limitations, primarily when particularly large perturbations are considered. While (7) provides a improvement over the linear phase and isostable reduced equations, it is only accurate to first order in the isostable coordinates. Previous authors have developed strategies for computation of higher order approximation of the phase coordinates (e.g., the terms of the Hessian and beyond) near the periodic orbit [43], [44], however strategies are practically difficult to implement beyond second order accuracy, and can only be used to characterize perturbations starting from the limit cycle.

Below, a strategy is presented for computation of a reduced set of equations of the form

$$\begin{aligned} \dot{\theta} &= \omega + \mathcal{Z}(\theta, \psi_1, \ldots, \psi_M) \cdot U(t), \\ \dot{\psi}_j &= \kappa_j \psi_j + \mathcal{I}_j(\theta, \psi_1, \ldots, \psi_M) \cdot U(t), \quad j = 1, \ldots, M \\ x(\theta, \psi_1, \ldots, \psi_M) &= x^\gamma(\theta) + \mathcal{G}(\theta, \psi_1, \ldots, \psi_M), \end{aligned} \tag{9}$$

which can be determined to arbitrary orders of accuracy in the isostable coordinates. The necessary terms of (9) can be identified using an asymptotic expansion of the gradient of the phase and isostable coordinates near $x^\gamma(\theta)$. Ultimately, the required terms can be calculated by solving equations with computational complexity similar to (8) which is already used in the computation of standard phase reductions.

3.1 Asymptotic Expansion in Terms of Phase and Isostable Coordinates

Before computing asymptotic expansions of the phase and isostable coordinates near the periodic orbit, a higher order expansion of $x(\theta, \psi_1, \ldots, \psi_M)$ of the form:

$$\begin{aligned} \Delta x &\approx \sum_{k=1}^{M} \left[\psi_k g^k(\theta)\right] + \sum_{j=1}^{M}\sum_{k=1}^{j} \left[\psi_j \psi_k g^{jk}(\theta)\right] + \sum_{i=1}^{M}\sum_{j=1}^{i}\sum_{k=1}^{j} \left[\psi_i \psi_j \psi_k g^{ijk}(\theta)\right] + \ldots \\ &= \mathcal{G}(\theta, \psi_1, \ldots, \psi_M) \end{aligned} \tag{10}$$

must be obtained, where $\Delta x \equiv x(\theta, \psi_1, \ldots, \psi_M) - x^\gamma(\theta)$. Here, each $g^{ijk\cdots}(\theta)$ is analogous to the Floquet eigenfunctions $g^k(\theta)$ defined earlier in (5) and provide higher order corrections to Δx. In the above equation, while there are $N-1$ possible isostable coordinates, it is assumed that some of these coordinates decay rapidly so that only $M < N-1$ isostable coordinates need to be considered. Intuitively, (10) is an asymptotic expansion of x on a hypersurface for which $\psi_k = 0$ for $k > M$. The goal of this section will be to compute the necessary terms of $\mathcal{G}(\theta, \psi_1, \ldots, \psi_M)$

in the expansion (10) from which high-accuracy approximations for the gradients of the phase and isostable coordinates can be obtained.

To begin, assuming for the moment that $U(t) = 0$ so that $\dot{\theta} = \omega$ and $\dot{\psi}_k = \kappa_k \psi$, taking the time derivative of (10) yields

$$\frac{d\Delta x}{dt} = \sum_{k=1}^{M} \left[\frac{dg^k}{d\theta} \omega \psi_k + g^k \kappa_k \psi_k \right] + \sum_{j=1}^{M} \sum_{k=1}^{j} \left[\frac{dg^{jk}}{d\theta} \omega \psi_j \psi_k + g^{jk} (\kappa_j + \kappa_k) \psi_j \psi_k \right] + \sum_{i=1}^{M} \sum_{j=1}^{i} \sum_{k=1}^{j} \left[\frac{dg^{ijk}}{d\theta} \omega \psi_i \psi_j \psi_k + g^{ijk} (\kappa_i + \kappa_j + \kappa_k) \psi_i \psi_j \psi_k \right] + \dots . \tag{11}$$

Above, the θ dependence on the g functions has been dropped for convenience of notation. Noting that $\theta(t) = \theta(0) + \omega t$ so that $\omega = d\theta/dt$, one can rewrite (12) as

$$\frac{d\Delta x}{dt} = \sum_{k=1}^{M} \left[\frac{dg^k}{dt} \psi_k + g^k \kappa_k \psi_k \right] + \sum_{j=1}^{M} \sum_{k=1}^{j} \left[\frac{dg^{jk}}{dt} \psi_j \psi_k + g^{jk} (\kappa_j + \kappa_k) \psi_j \psi_k \right] + \sum_{i=1}^{M} \sum_{j=1}^{i} \sum_{k=1}^{j} \left[\frac{dg^{ijk}}{dt} \psi_i \psi_j \psi_k + g^{ijk} (\kappa_i + \kappa_j + \kappa_k) \psi_i \psi_j \psi_k \right] + \dots . \tag{12}$$

Simultaneously, an expansion of (1) will be considered taking $U(t) = 0$. Let $F(x) = \begin{bmatrix} f_1(x) & \dots & f_N(x) \end{bmatrix}^T$. The notation from [45] will be used below where $\otimes$ denotes the Kronecker product and $\mathrm{vec}(\cdot)$ is an operator that stacks each column of a matrix to form a single column vector. Letting $f_j^{(0)}(\theta)$ denote the evaluation of $f_j(x)$ at $x(\theta)$, a series of matrices comprised of partial derivatives will be defined recursively as

$$f_j^{(k)}(\theta) = \frac{\partial \mathrm{vec}\left(f_j^{(k-1)}\right)}{\partial x^T} \in \mathbb{R}^{N^{(k-1)} \times N}, \tag{13}$$

where all partial derivatives are evaluated at $x(\theta)$ on the limit cycle. With this information, and using the relationship $\mathrm{vec}(ABC) = (C^T \otimes A)\mathrm{vec}(B)$ [45], a Taylor expansion of f_j centered at $x(\theta)$ is obtained:

$$f_j(x(\theta) + \Delta x) = f_j(\theta) + f_j^{(1)}(\theta)\Delta x + \sum_{i=2}^{\infty} \frac{1}{i!} \left[\overset{i}{\otimes} \Delta x^T \right] \mathrm{vec}(f_j^{(i)}(\theta)), \tag{14}$$

where, for example, $\left[\overset{3}{\otimes} \Delta x^T \right] = \Delta x^T \otimes \Delta x^T \otimes \Delta x^T \in \mathbb{R}^{1 \times N^3}$. Substituting the expansion (14) into

(1) one finds

$$\frac{d\Delta x}{dt} = J\Delta x + \begin{bmatrix} \sum_{i=2}^{\infty} \frac{1}{i!} \left[\overset{i}{\otimes} \Delta x^T \right] \mathrm{vec}(f_1^{(i)}(\theta)) \\ \vdots \\ \sum_{i=2}^{\infty} \frac{1}{i!} \left[\overset{i}{\otimes} \Delta x^T \right] \mathrm{vec}(f_N^{(i)}(\theta)) \end{bmatrix}$$
$$= J \left[\sum_{k=1}^{M} \left[\psi_k g^k(\theta) \right] + \sum_{j=1}^{M} \sum_{k=1}^{j} \left[\psi_j \psi_k g^{jk}(\theta) \right] + \dots \right]$$
$$+ \begin{bmatrix} \sum_{i=2}^{\infty} \frac{1}{i!} \left[\overset{i}{\otimes} \left[\sum_{k=1}^{M} \left[\psi_k g^k(\theta) \right] + \sum_{j=1}^{M} \sum_{k=1}^{j} \left[\psi_j \psi_k g^{jk}(\theta) \right] + \dots \right]^T \right] \mathrm{vec}(f_1^{(i)}(\theta)) \\ \vdots \\ \sum_{i=2}^{\infty} \frac{1}{i!} \left[\overset{i}{\otimes} \left[\sum_{k=1}^{M} \left[\psi_k g^k(\theta) \right] + \sum_{j=1}^{M} \sum_{k=1}^{j} \left[\psi_j \psi_k g^{jk}(\theta) \right] + \dots \right]^T \right] \mathrm{vec}(f_N^{(i)}(\theta)) \end{bmatrix}, \quad (15)$$

where J is the Jacobian of the vector field F evaluated at $x(\theta)$. Equations (15) and (12) are equivalent, and relationships between each of the g functions of the expansion can be obtained by finding terms with matching powers in the isostable coefficients in the two equations. For example, matching all terms that are proportional to ψ_k yields the relationships:

$$\frac{dg^k}{dt} = (J - \kappa_k \mathrm{Id}) g^k(\theta), \ k = 1, \dots, M. \quad (16)$$

Matching all terms that are proportional to two isostable coordinates (i.e., $\psi_k \psi_j$) yields

$$\frac{dg^{jk}}{dt} = (J - (\kappa_j + \kappa_k)\mathrm{Id}) g^{jk}(\theta) + \frac{1}{\eta} \begin{bmatrix} {g^j}^T H_1 g^k \\ \vdots \\ {g^j}^T H_N g^k \end{bmatrix}, \quad (17)$$

where H_i denotes the Hessian of f_i and $\eta = 1$ if $j \neq k$ and $\eta = 2$ otherwise. Each of the Hessian terms in (17) are evaluated at $x(\theta)$. Relationships for higher order terms (i.e., $g_{ijk}(\theta)$) can also be found by matching powers of each of the ψ_k terms in (15) and (12). This task can be accomplished using a symbolic computational package. A particularly useful pattern that emerges is shown below:

$$\frac{dg^{ijk\dots}}{dt} = (J - (\kappa_i + \kappa_j + \kappa_k + \dots)\mathrm{Id}) g^{ijk\dots}(\theta) + q^{ijk\dots}(\theta), \quad (18)$$

where $q^{ijk\dots}(\theta)$ is comprised only of terms from lower terms of the expansion (for example, $q_{321}(\theta)$ will only be a function of terms including $g^1(\theta), g^{21}(\theta), g^{31}(\theta)$, etc., but will not contain terms such as $g^{111}(\theta)$).

3.1.1 A Brief Note on Computation and Non-Uniqueness of the Functions in the State Expansion

Since J is evaluated on the periodic orbit, Equation (16) is a linear, periodic equation and $g^k(\theta)$ is its periodic solution. The equation $\dot{g}^k = J(t)g^k$ has a Floquet exponent of κ_k and so $\dot{g}^k = (J(t) - \kappa_k \mathrm{Id})g^k$ has a Floquet exponent of 0 and normalization will be required. For all first order

terms the normalization $w_k^T g^k(0) = 1$ will be used, where w_k is a left eigenvector of the fundamental matrix of (4) associated with the eigenvalue $\lambda_k = \exp(\kappa_k T)$.

The general structure of (18) provides a strategy for computation of the individual terms of the expansion. To begin, all first order terms can be computed by finding the appropriately normalized periodic solutions to (16). Once all lower order terms of the expansion have been calculated, one can move on to compute higher order terms to arbitrary order accuracy. The expansion (10) resulting from this procedure will not be unique in some instances. To illustrate how this can occur, consider an expansion of (1) using two isostable coordinates with Floquet multipliers $\kappa_1 = -0.25$ and $\kappa_2 = -0.5$. When computing g^{11} according to (17), noting that $2\kappa_1 = \kappa_2$, one finds

$$\frac{dg^{11}}{dt} = (J - \kappa_2 \mathrm{Id})g^{11} + \frac{1}{2}\begin{bmatrix} {g^1}^T H_1 g^1 \\ \vdots \\ {g^1}^T H_N g^1 \end{bmatrix}. \tag{19}$$

Recalling $\frac{dg^{11}}{dt} = (J(t) - \kappa_2)g^{11}$ has a Floquet exponent of zero, the solution to (19) can be written as

$$g^{11}(\theta) = g^{11^*}(\theta) + \beta g^2(\theta), \tag{20}$$

where g^{11^*} is a particular solution to (19) and $\beta \in \mathbb{R}$ can be chosen arbitrarily. In general, an expansion (10) to order accuracy $\chi \in \mathbb{N}$ will not be unique if there exists some combination of $\alpha_k \in \mathbb{N}$ for which

$$\alpha_1\kappa_1 + \cdots + \alpha_M\kappa_M = \kappa_j, \tag{21}$$

with $\sum_{k=1}^M \alpha_k \leq \chi$.

3.2 Asymptotic Expansion and Computation of the Gradient of the Phase and Isostable Coordinates

Knowledge of the asymptotic expansion (10) allows for efficient computation of the gradient of the phase and isostable coordinates. To do so, one can start with an expansion of the gradient of the phase and isostable coordinates. Letting $\frac{\partial\theta}{\partial x}\big|_{x(\theta,\psi_1,\ldots,\psi_M)} \equiv \mathcal{Z}(\theta,\psi_1,\ldots,\psi_M)$ and $\frac{\partial\psi_n}{\partial x}\Big|_{x(\theta,\psi_1,\ldots,\psi_M)} \equiv \mathcal{I}_n(\theta,\psi_1,\ldots,\psi_M)$, one can write

$$\begin{aligned}
\mathcal{Z}(\theta,\psi_1,\ldots,\psi_M) &\approx Z(\theta) + \sum_{k=1}^{M}\left[\psi_k Z^k(\theta)\right] + \sum_{j=1}^{M}\sum_{k=1}^{j}\left[\psi_j\psi_k Z^{jk}(\theta)\right] + \sum_{i=1}^{M}\sum_{j=1}^{i}\sum_{k=1}^{j}\left[\psi_i\psi_j\psi_k Z^{ijk}(\theta)\right] + \ldots, \\
\mathcal{I}_n(\theta,\psi_1,\ldots,\psi_M) &\approx I_n(\theta) + \sum_{k=1}^{M}\left[\psi_k I_n^k(\theta)\right] + \sum_{j=1}^{M}\sum_{k=1}^{j}\left[\psi_j\psi_k I_n^{jk}(\theta)\right] + \sum_{i=1}^{M}\sum_{j=1}^{i}\sum_{k=1}^{j}\left[\psi_i\psi_j\psi_k I_n^{ijk}(\theta)\right] + \ldots.
\end{aligned} \tag{22}$$

In the above equation, $Z(\theta)$ and $I_n(\theta)$ represent the gradient of the phase and isostable coordinates evaluated on the periodic orbit; these terms also appear in (7). Likewise, $Z^k(\theta)$ and $I_j^k(\theta)$ are equivalent to the terms $B^k(\theta)$ and $C_j^k(\theta)$, respectively, from (7). Computation and utilization of these terms has been discussed previously in [28], [26]. Direct strategies for the computation of the remaining terms $Z^{ijk\cdots}(\theta)$ and $I_n^{ijk\cdots}(\theta)$ that provide higher order accuracy corrections have not previously been developed. In the derivations to follow, Sections 3.2.1 and 3.2.2 give equations similar in structure to (18) that can be used to compute each $Z^{ijk\cdots}(\theta)$ and $I_n^{ijk\cdots}(\theta)$. Section 3.2.3 provides an alternative strategy for computing the gradient of the phase and isostable coordinates directly from the relationship $x(\theta,\psi_1,\ldots,\psi_M) = x^\gamma(\theta) + \mathcal{G}(\theta,\psi_1,\ldots,\psi_M)$ which can be used under certain conditions.

3.2.1 Computing the Terms for the Gradient of the Phase

To begin, computation of the terms of $\mathcal{Z}$ will be considered. Consider any trajectory of (1) in the basin of attraction of the periodic orbit given by $x = x^\gamma(\theta) + \Delta x(\theta, \psi_1, \ldots, \psi_M)$. Also consider a perturbed trajectory x_1 which has been initially shifted by an infinitesimal amount $\Delta x = \mathcal{O}(\epsilon)$ where $0 < \epsilon \ll 1$. The shift in θ due to this initial perturbation is

$$\Delta\theta = \Delta x^T \mathcal{Z}(\theta, \psi_1, \ldots, \psi_M). \tag{23}$$

Taking the time derivative of (23) and noting that $d\Delta\theta/dt = 0$ in the absence of perturbation, one finds

$$0 = \frac{d\Delta x}{dt}^T \mathcal{Z} + \Delta x^T \frac{d\mathcal{Z}}{dt}. \tag{24}$$

Note that explicit dependence of $\mathcal{Z}$ on the phase and isostable coordinates has been dropped for notational convenience. Because Δx is small, one can use Taylor expansion to write

$$\frac{d\Delta x}{dt} = \left.\frac{\partial F}{\partial x}\right|_x \Delta x + \mathcal{O}(\epsilon^2). \tag{25}$$

Substituting this result into (24), neglecting $\mathcal{O}(\epsilon^2)$ terms, and rearranging yields

$$0 = \Delta x^T \left[\left.\frac{\partial F}{\partial x}\right|_x^T \mathcal{Z} + \frac{d\mathcal{Z}}{dt} \right]. \tag{26}$$

Since Δx is arbitrary, it follows that the terms inside the brackets of (26) must be equal to zero and thus

$$\frac{d\mathcal{Z}}{dt} = -\left.\frac{\partial F}{\partial x}\right|_x^T \mathcal{Z}. \tag{27}$$

While the above derivation mirrors the derivation of the adjoint equation (8) from [40], this derivation significantly expands on it by considering a nominal trajectory x that has already been perturbed from the periodic orbit.

Let $J^T \equiv \frac{\partial F}{\partial x}^T = \begin{bmatrix} \frac{\partial f_1}{\partial x}^T & \ldots & \frac{\partial f_N}{\partial x}^T \end{bmatrix}$, where all partial derivatives are evaluated along the periodic orbit. Along a specific trajectory near the periodic orbit, it is possible to write an asymptotic expansion

$$\begin{aligned} \left.\frac{\partial F}{\partial x}\right|_{x^\gamma+\Delta x}^T &= J^T + \begin{bmatrix} a_1 & \cdots & a_N \end{bmatrix}, \\ a_i &= \sum_{j=1}^{\infty} \frac{1}{j!} \left(\left[\overset{j}{\otimes} \Delta x^T \right] \otimes \mathrm{Id} \right) \mathrm{vec}(f_i^{(j+1)}), \end{aligned} \tag{28}$$

where a_i is a column vector and $f_i^{(i+1)}$ was defined in (13). Recalling that $d\psi_k/dt = \kappa_k \psi_k$, time derivatives of (22) can also be readily written in powers of the isostable coordinates

$$\begin{aligned} \frac{d\mathcal{Z}}{dt} = \frac{dZ}{dt} &+ \sum_{k=1}^{M} \psi_k \left[\kappa_k Z^k(\theta) + \frac{dZ^k}{dt} \right] + \sum_{j=1}^{M} \sum_{k=1}^{j} \psi_j \psi_k \left[(\kappa_j + \kappa_k) Z^{jk} + \frac{dZ^{jk}}{dt} \right] \\ &+ \sum_{i=1}^{M} \sum_{j=1}^{i} \sum_{k=1}^{j} \psi_i \psi_j \psi_k \left[(\kappa_i + \kappa_j + \kappa_k) Z^{ijk} + \frac{dZ^{ijk}}{dt} \right] + \ldots. \end{aligned} \tag{29}$$

Noticing that equations (27) and (29) are identical, one can write

$$\frac{dZ}{dt} + \sum_{k=1}^{M} \psi_k \left[\kappa_k Z^k(\theta) + \frac{dZ^k}{dt} \right] + \sum_{j=1}^{M} \sum_{k=1}^{j} \psi_j \psi_k \left[(\kappa_j + \kappa_k) Z^{jk}(\theta) + \frac{dZ^{jk}}{dt} \right] + \cdots =$$
$$- \left[J^T + \begin{bmatrix} a_1 & \cdots & a_N \end{bmatrix} \right] \left(Z(\theta) + \sum_{k=1}^{M} \left[\psi_k Z^k(\theta) \right] + \sum_{j=1}^{M} \sum_{k=1}^{j} \left[\psi_j \psi_k Z^{jk}(\theta) \right] + \dots \right), \tag{30}$$

where equations $\mathcal{Z}$ from (22) and $\frac{\partial F}{\partial x}^T|_{x^\gamma + \Delta x}$ from (28) are substituted into the appropriate locations in (27). Finally, relationships for each of the terms in the expansions (22) can be obtained by matching coefficients in orders of each of the isostable coordinates in (30). For instance, matching terms up to second order accuracy in the isostable coordinate ψ_j yields

$$\psi_j^0 : \frac{dZ}{dt} = -J^T Z(\theta), \tag{31}$$

$$\psi_j^1 : \frac{dZ^j}{dt} = -(J^T + \kappa_j \mathrm{Id}) Z^j(\theta) - \sum_{i=1}^{N} \left[e_i^T Z(\theta) \left((g^j(\theta))^T \otimes \mathrm{Id} \right) \mathrm{vec}(f_i^{(2)}) \right], \tag{32}$$

$$\psi_j^2 : \frac{dZ^{jj}}{dt} = -(J^T + 2\kappa_j \mathrm{Id}) Z^{jj}(\theta) - \sum_{i=1}^{N} \Bigg[e_i^T Z^j(\theta) \left((g^j(\theta))^T \otimes \mathrm{Id} \right) \mathrm{vec}(f_i^{(2)})$$
$$+ \frac{1}{2} e_i^T Z(\theta) \left((g^j(\theta))^T \otimes (g^j(\theta))^T \otimes \mathrm{Id} \right) \mathrm{vec}(f_i^{(3)}) \Bigg], \tag{33}$$

where e_i is the i^{th} element of the standard unit basis. Matching higher order powers of the appropriate isostable coordinates in (30) can be accomplished efficiently with a symbolic computational package. Much like when computing the relationships for the terms of (10), equations for the higher order terms of the phase response equation follow the pattern

$$\frac{dZ^{ijk\dots}}{dt} = -(J^T + (\kappa_i + \kappa_j + \kappa_k + \dots)\mathrm{Id}) Z^{ijk\dots}(\theta) + q_\theta^{ijk\dots}(\theta), \tag{34}$$

where $q_\theta^{ijk\dots}$ is comprised of only lower order terms of the expansion of $\mathcal{Z}(\theta, \psi_1, \dots, \psi_M)$, (e.g., $q_\theta^{113}(\theta)$ can contain terms from $Z^1(\theta)$ and $Z^{13}(\theta)$ but will not contain terms such as $Z^{111}(\theta)$). The terms of the expansion $Z(\theta)$, $Z^j(\theta)$, and $Z^{jj}(\theta)$ are the periodic solutions to (31), (32), and (33), respectively. All higher order terms can be obtained by computing periodic solutions to equations of the form (34). Due to the general structure of (34), all terms of the expansion can be obtained by first solving for the lowest order terms, and successively moving to higher order terms.

In the above derivation, Equation (8) is the standard adjoint equation (derived e.g., in [40]) which gives the local gradient of the phase coordinates along the periodic orbit. Noting that $f_i^{(2)}$ is simply the Hessian of f_i, Equation (32) was previously derived in [28]. Using the strategy detailed above, it is straightforward to derive relationships for all other higher order corrections to the phase reduction; relations of these higher order corrections have not been previously obtained.

3.2.2 Computing the Terms of the Gradient of the Isostable Coordinates

Equations for computing the terms of the isostable reduction are very similar to those of the form (34). To derive these equations, once again consider any trajectory of (1) in the basin of attraction

of the periodic orbit given by $x = x^\gamma(\theta) + \Delta x(\theta, \psi_1, \ldots, \psi_M)$. Also consider a perturbed trajectory x_1 which has been initially shifted by an infinitesimal amount $\Delta x = \mathcal{O}(\epsilon)$ where $0 < \epsilon \ll 1$. The shift in ψ_n due to this initial perturbation is

$$\Delta\psi_n = \Delta x^T \mathcal{I}_n(\theta, \psi_1, \ldots, \psi_M). \tag{35}$$

Taking the time derivative of (35) yields

$$\kappa_n \Delta\psi_n = \frac{d\Delta x}{dt}^T \mathcal{I}_n + \Delta x^T \frac{d\mathcal{I}_n}{dt}, \tag{36}$$

which can be manipulated to give

$$0 = -\kappa_n \Delta x^T \mathcal{I}_n + \frac{d\Delta x}{dt}^T \mathcal{I}_n + \Delta x^T \frac{d\mathcal{I}_n}{dt}. \tag{37}$$

Substituting the Taylor expansion from (25) into (37) gives

$$0 = \Delta x^T \left[\left(\frac{\partial F}{\partial x}^T \bigg|_x - \kappa_n \mathrm{Id} \right) \mathcal{I}_n + \frac{d\mathcal{I}_n}{dt} \right]. \tag{38}$$

Once again, since Δx is arbitrary, the terms inside the brackets of (38) must be zero so that

$$\frac{d\mathcal{I}_n}{dt} = -\left(\frac{\partial F}{\partial x}^T \bigg|_x - \kappa_n \mathrm{Id} \right) \mathcal{I}_n. \tag{39}$$

Equation (38) is nearly identical in structure to (27) except for the extra term $\kappa_n \mathrm{Id}$. Repeating the arguments from the previous section, one can Taylor expand (39) in powers of the isostable coordinates to yield

$$\begin{aligned} \frac{dI_n}{dt} + \sum_{k=1}^{M} \psi_k \left[\kappa_k I_n^k(\theta) + \frac{dI_n^k}{dt} \right] + \sum_{j=1}^{M} \sum_{k=1}^{j} \psi_j \psi_k \left[(\kappa_j + \kappa_k) I_n^{jk}(\theta) + \frac{dI_n^{jk}}{dt} \right] + \cdots = \\ - \left[J^T + \begin{bmatrix} a_1 & \cdots & a_N \end{bmatrix} - \kappa_n \mathrm{Id} \right] \left(I_n(\theta) + \sum_{k=1}^{M} \left[\psi_k I_n^k(\theta) \right] + \sum_{j=1}^{M} \sum_{k=1}^{j} \left[\psi_j \psi_k I_n^{jk}(\theta) \right] + \ldots \right). \end{aligned} \tag{40}$$

Once again, matching coefficients in orders of each isostable coordinate from Equation (40) yields relationships that can be used to compute the terms of the isostable coordinate expansion from (22). For instance, matching terms up to second order accuracy in ψ_j one finds

$$\psi_j^0 : \frac{dI_n}{dt} = -(J^T - \kappa_n \mathrm{Id}) I_n(\theta), \tag{41}$$

$$\psi_j^1 : \frac{dI_n^j}{dt} = -(J^T + (\kappa_j - \kappa_n)\mathrm{Id}) I_n^j(\theta) - \sum_{i=1}^{M} \left[e_i^T I_n(\theta) \left((g^j(\theta))^T \otimes \mathrm{Id} \right) \mathrm{vec}(f_i^{(2)}) \right], \tag{42}$$

$$\begin{aligned} \psi_j^2 : \frac{dI_n^{jj}}{dt} = -(J^T + (2\kappa_j - \kappa_n)\mathrm{Id}) I_n^{jj}(\theta) - \sum_{i=1}^{M} \Bigg[e_i^T I_n^j(\theta) \left((g^j(\theta))^T \otimes \mathrm{Id} \right) \mathrm{vec}(f_i^{(2)}) \\ + \frac{1}{2} e_i^T I_n(\theta) \left((g^j(\theta))^T \otimes (g^j(\theta))^T \otimes \mathrm{Id} \right) \mathrm{vec}(f_i^{(3)}) \Bigg]. \end{aligned} \tag{43}$$

As before, matching powers of the appropriate isostable coordinates to obtain equations for higher order relationships of the expansion of the isostable response curve can be performed using a symbolic computational package. Once again, the general pattern for the isostable response equations follows

$$\frac{dI_n^{ijk\dots}}{dt} = -(J^T + (-\kappa_n + \kappa_i + \kappa_j + \kappa_k + \dots)\mathrm{Id})I_n^{ijk\dots}(\theta) + q_{\psi_n}^{ijk\dots}(\theta), \tag{44}$$

where $q_{\psi_n}^{ijk\dots}(\theta)$, is comprised of only lower terms of the expansion of $\mathcal{I}_n(\theta, \psi_1, \dots, \psi_M)$. The terms of the expansion $I_n(\theta)$, $I_n^j(\theta)$, and $I_n^{jj}(\theta)$ can be obtained by computing periodic solutions to (41), (42), (43), respectively. All other terms can be found by computing the periodic solutions to equations of the form (44).

The relationships (41) and (42) were previously derived in [25] and [28], respectively. The above strategy allows for straightforward derivation for the relationships governing even higher order corrections to the isostable reduced equations using (44) and can be obtained with a symbolic computational package. These higher order relationships have not been obtained previously.

A Brief Note on Normalization of the Terms of the Phase and Isostable Response Expansion

Usually, the periodic solutions of (34) and (44) are uniquely determined, however, for certain terms of the expansion, additional normalization will be required. For example, consider any term of the form $I_j^j(\theta)$. Using (44) one finds

$$\frac{dI_j^j}{dt} = -J^T I_j^j(\theta) + q_{\psi_j}^j(\theta). \tag{45}$$

Noting that (45) can be viewed as a periodically forced version of the adjoint equation (31) used in the computation of $Z(\theta)$, periodic solutions of (45) can be written as

$$I_j^j(\theta) = I_j^{j*}(\theta) + \beta Z(\theta), \tag{46}$$

where $I_j^{j*}(\theta)$ is a particular solution and β is an arbitrary constant. In this case, additional normalization is necessary. To do so, recall from the definition of phase (resp., isostable) coordinates, that $\frac{d\theta}{dt} = \omega$ (resp., $\frac{d\psi_n}{dt} = \kappa_n \psi_n$) in the absence of perturbations. Therefore, a normalizing condition can be obtained from the relation

$$\omega = \left(\frac{\partial \theta}{\partial x}\right)^T \frac{dx}{dt} = \left[Z(\theta) + \sum_{k=1}^{M}\left[\psi_k Z^k(\theta)\right] + \sum_{j=1}^{M}\sum_{k=1}^{j}\left[\psi_j \psi_k Z^{jk}(\theta)\right] + \dots\right]^T \left[F(x^\gamma(\theta)) + \frac{d\Delta x}{dt}\right], \tag{47}$$

$$\kappa_n \psi_n = \left(\frac{\partial \psi_n}{\partial x}\right)^T \frac{dx}{dt} = \left[I_n(\theta) + \sum_{k=1}^{M}\left[\psi_k I_n^k(\theta)\right] + \sum_{j=1}^{M}\sum_{k=1}^{j}\left[\psi_j \psi_k I_n^{jk}(\theta)\right] + \dots\right]^T \left[F(x^\gamma(\theta)) + \frac{d\Delta x}{dt}\right]. \tag{48}$$

By substituting (15) into (47) and (48), one finds a normalization condition for the terms of the expansion of the phase response curve by matching powers of the isostable coordinates. For instance, matching terms to leading order ψ_j in (48) yields the normalizing condition $I_j(\theta)^T J g^j(\theta) + I_j^j(\theta)^T F(x^\gamma(\theta)) = \kappa_j$ providing a necessary normalization for (46).

3.2.3 Inference of the Expansion for the Gradient of the Phase and Isostable Coordinates Directly From the State Expansion

Section 3.2 illustrates a strategy for computing all of the terms of $\mathcal{Z}$ and $\mathcal{I}_j$ to arbitrary accuracy in the isostable coordinates for use in the reduction (9). For certain systems, it is possible to infer the terms $\mathcal{Z}$, and $\mathcal{I}_j$ directly from the relationship $x(\theta,\psi_1,\ldots,\psi_M) = x^\gamma(\theta)+\mathcal{G}(\theta,\psi_1,\ldots,\psi_M)$ thereby bypassing the need to compute the terms of the asymptotic expansion (22) directly. As explained below, this strategy is generally only applicable for particularly small values of $\psi_1,\ldots,\psi_M$.

To begin, recall that in the reduction (9) it is assumed that ψ_j is well approximated by zero for $j > M$, i.e., the relation $x(\theta)+\mathcal{G}(\theta,\psi_1,\ldots,\psi_M)$ gives a hypersurface for which $\psi_j = 0$ for $j > M$. Letting $x_0 = \begin{bmatrix} x_1 & \ldots & x_N \end{bmatrix}^T$ be any initial condition on this hypersurface with corresponding phase and isostable coordinates $\theta,\psi_1,\ldots,\psi_M$, any infinitesimal perturbation Δx from this initial condition can be represented to leading order according to

$$\Delta x = A_\Psi \Delta\Psi, \tag{49}$$

where $\Delta\Psi \equiv \begin{bmatrix}\Delta\theta & \Delta\psi_1 & \ldots & \Delta\psi_{N-1}\end{bmatrix}^T$ and

$$A_\Psi \equiv \left[\left(\tfrac{\partial x^\gamma}{\partial\theta}+\tfrac{\partial\mathcal{G}}{\partial\theta}\right) \quad \tfrac{\partial\mathcal{G}}{\partial\psi_1} \quad \ldots \quad \tfrac{\partial\mathcal{G}}{\partial\psi_M} \quad g^{M+1}(\theta) \quad \ldots \quad g^N(\theta)\right] \in \mathbb{R}^{N\times N}, \tag{50}$$

with all partial derivatives evaluated at $\theta,\psi_1,\ldots,\psi_M$. Recall here that each $g^j(\theta)$ is a Floquet eigenfunction of (4). While the reduction (9) does not explicitly include contributions from $g^{M+1}(\theta),\ldots,g^N(\theta)$, they are necessary here to allow for perturbations Δx in any direction. Provided the inverse of A_Ψ as given by (50) exists, the change in phase and isostable coordinates is given by

$$A_\Psi^{-1}\Delta x = \Delta\Psi. \tag{51}$$

Recall that $\mathcal{Z}(\theta,\psi_1,\ldots,\psi_M)$ and $\mathcal{I}_j(\theta,\psi_1,\ldots,\psi_M)$ are simply approximations of the gradient of the phase and isostable coordinates, respectively. Therefore, the rows of A_Ψ^{-1} correspond directly to $\mathcal{Z}$ and $\mathcal{I}_j$ according to

$$\begin{aligned}\mathcal{Z}(\theta,\psi_1,\ldots,\psi_M) &= (e_1^T A_\Psi^{-1})^T,\\ \mathcal{I}_j(\theta,\psi_1,\ldots,\psi_M) &= (e_{j+1}^T A_\Psi^{-1})^T.\end{aligned} \tag{52}$$

The condition number of A_Ψ becomes an important consideration when computing the phase and isostable response curves using (52). For any θ, when $\psi_1 = \psi_2 = \cdots = \psi_M = 0$, i.e., for states on the periodic orbit, A_Ψ is always invertible with

$$\left(A_\Psi|_{\psi_1=\psi_2=\cdots=\psi_M=0}\right)^{-1} = \begin{bmatrix} Z_1(\theta) & I_1(\theta) & \ldots & I_N(\theta)\end{bmatrix}^T. \tag{53}$$

The above relationship follows from (A2), (A7), and (A8) in Appendix A. As the isostable coordinates increase, taking this matrix inverse can amplify the effects of numerical error when A_Ψ is ill conditioned and ultimately can prohibit the computation of the gradient of phase of the isostable coordinates. To illustrate this, let

$$\begin{aligned}A_\Psi &= \left[\left(\tfrac{\partial x^\gamma}{\partial\theta}+\tfrac{\partial G}{\partial\theta}\right) \quad g^1(\theta) \quad \ldots \quad g^N(\theta)\right] + \left[0 \quad \left(\tfrac{\partial\mathcal{G}}{\partial\psi_1}-g^1(\theta)\right) \quad \ldots \quad \left(\tfrac{\partial\mathcal{G}}{\partial\psi_M}-g^M(\theta)\right) \quad 0 \quad \ldots \quad 0\right]\\ &= A+E.\end{aligned} \tag{54}$$

In (54), the matrix A represents A_Ψ when evaluated on the periodic orbit, and E represents a small perturbation for nonzero isostable coordinates. Rewriting the perturbation as

$$\begin{aligned} E &= \begin{bmatrix} 0 & \left(\frac{\partial \mathcal{G}}{\partial \psi_1} - g^1(\theta)\right) & \dots & \left(\frac{\partial \mathcal{G}}{\partial \psi_M} - g^M(\theta)\right) \end{bmatrix} \mathrm{Id}_{M\times M} \begin{bmatrix} \mathrm{Id}_{M\times M} & \mathbb{0}_{M\times N-M} \end{bmatrix} \\ &= WDV, \end{aligned} \tag{55}$$

where $\mathrm{Id}_{M\times M}$ and $\mathbb{0}_{M\times N-M}$ represent the identity matrix and a matrix of zeros, respectively, with the size specified. Starting with the Sherman-Morrison-Woodbury matrix identity [46], one finds

$$\begin{aligned} (A+E)^{-1} &= (A+WDV)^{-1} \\ &= A^{-1} - A^{-1}W(\mathrm{Id} + VA^{-1}W)^{-1}VA^{-1} \\ &= A^{-1} - A^{-1}W\left(\sum_{j=0}^{\infty}(-VA^{-1}W)^j\right)VA^{-1} \\ &= A^{-1} + A^{-1}\sum_{j=1}^{\infty}(-EA^{-1})^j, \end{aligned} \tag{56}$$

where the third line uses the relationship $(\mathrm{Id}-P)^{-1} = \mathrm{Id} + \sum_{j=1}^{\infty} P^n$ which is valid for small matrix perturbations P, and the fourth line follows from direct simplification. From (56) it is immediately apparent how (52) can fail to accurately provide the correct relationships for the desired functions. Foremost, if the condition number of A_Ψ (i.e., the ratio of the largest and smallest singular values) grows too large, numerical issues will arise when computing the matrix inverse as part of (52). The computation will suffer if at a given value of θ the condition number of $A = A_\Psi|_{\psi_1=\psi_2=\dots=\psi_M=0}$ is large. In (56), $(A+E)^{-1}$ can be approximated to n^{th} order accuracy in the isostable coordinates by taking the infinite sum to n terms (provided that $\mathcal{G}$ is also approximated to at least n^{th} order in the isostable coordinates). If the condition number of A^{-1} is particularly large, this will also result in significant error in the numerical computation. This relationship can be clearly seen in results from Figure 5 for an example system.

As a final note, because the final $N-M-1$ columns of the matrix A_Ψ are not used in the reduction (9), the terms $g^{M+1}(\theta), \dots, g^N(\theta)$ do not need to be explicitly computed. Instead, by noting that the set $\{g^{M+1}(\theta), \dots, g^N(\theta)\}$ spans the orthogonal complement of $\{Z_1(\theta), I_1(\theta), \dots, I_M(\theta)\}$, one can simply compute the orthogonal complement of $\{Z_1(\theta), I_1(\theta), \dots, I_M(\theta)\}$ and use it to replace $g^{M+1}(\theta), \dots, g^N(\theta)$ from (50). It is straightforward to show that the first $M+1$ rows of A_Ψ remain unchanged with this modification.

In summary, $\mathcal{Z}$ and each $\mathcal{I}_j$ can be computed to high-order accuracy using (52), but the requirement of taking the matrix inverse will lead to numerical issues when large isostable coordinates are considered. Generally, it is better to compute $\mathcal{Z}$ and each $\mathcal{I}_j$ using strategies described in Section 3.2.

4 Patchwork Phase-Amplitude Reduction

The methods detailed in the previous section can be used to identify phase-amplitude reduced equations with respect to a single periodic orbit. In some situations it can be useful to consider a reduction based on multiple periodic orbits obtained with different choices of nominal parameters. To illustrate this idea, consider the differential equation

$$\frac{dx}{dt} = F(x, p_0) + U(t), \tag{57}$$

where $x \in \mathbb{R}^N$ is the state, $F(x,p)$ gives the unperturbed dynamics where $p \in \mathbb{R}$ is a parameter, $p = p_0$ is the nominal value of this parameter, and $U(t)$ is a time dependent input. Here, Equation (57) is identical to (1) except for the explicit dependence on the parameter p. For any value of p, one can rewrite (57) as

$$\frac{dx}{dt} = F(x,p) + U_p(x,p,t) \tag{58}$$

where $U_p(x,p,t) \equiv F(x,p_0) - F(x,p) + U(t)$. Intuitively, Equation (58) illustrates that Equation (57) can be analyzed with respect to any periodic orbit x_p^γ from the dynamical system $\dot{x} = F(x,p)$ as long as the effective input U_p is defined appropriately. In general, the asymptotic expansion (9) from the previous section works well provided the isostable coordinates are small in magnitude. The so-called patchwork phase-amplitude reduction proposed here actively switches between nominal periodic orbits as necessary to keep the isostable coordinates small.

4.1 Level Sets of Isostable Coordinates of Nearby Periodic Orbits

To begin, it will be necessary to show that the level sets of isostable coordinates are similar between nearby periodic orbits. Let $x_{p_1}^\gamma(\theta)$ and $x_{p_2}^\gamma(\theta)$ be stable periodic orbits obtained when $p = p_1$ and $p = p_2 = p_1 + \Delta p$, respectively, where Δp is an $\mathcal{O}(\epsilon)$ term. For the patchwork reduction considered here, it will be assumed that all but one of the $N-1$ Floquet exponents associated with decay in directions transverse to the periodic orbit are small so that the dynamical behavior can be well-characterized with a single isostable coordinate. Let θ^{p_1} and $\psi_1^{p_1}$ (resp., θ^{p_2} and $\psi_1^{p_2}$) be the phase and isostable coordinates associated with the orbit $x_{p_1}^\gamma$ (resp., $x_{p_2}^\gamma$).

Using (9), one can represent the perturbed dynamical behavior near either of these periodic orbits as

$$\begin{aligned}
\dot{\theta}^q &= \omega^q + \mathcal{Z}^q(\theta^q, \psi_1^q) \cdot U_p(x,q,t), \\
\dot{\psi}_1^q &= \kappa_1^q \psi_1^q + \mathcal{I}_1^q(\theta^q, \psi_1^q) \cdot U_p(x,q,t), \\
x(\theta^q, \psi_1^q) &= x_q^\gamma(\theta^q) + \mathcal{G}^q(\theta^q, \psi_1^q),
\end{aligned} \tag{59}$$

where $q = \{p_1, p_2\}$ is used to denote the functions and coordinates associated with periodic orbits taking $p_1 = q$ or $p_2 = q$. The analysis to follow shows that for any value of θ there exists some isostable coordinate α for which $x_{p_1}(\theta) + \mathcal{G}^{p_1}(\theta,\alpha) \approx x_{p_2}(\theta) + \mathcal{G}^{p_2}(\theta,-\alpha)$, so that the level sets of the isostable coordinates are approximately identical. At these locations, it is possible to recompute the phase and isostable coordinates of one orbit in terms of the other orbit. Ultimately, this makes it possible choose the orbit with the lower isostable coordinates to limit the error in the resulting reduction. This general idea is highlighted in Figure 1. The patchwork phase-amplitude reduction proposed here can be performed by taking a large collection of orbits and actively switching between them.

To continue, the phase and isostable dynamics of the periodic orbit resulting from $\dot{x} = F(x,q)$ will be analyzed in response to a static parameter perturbation. For the moment U_p will be taken to be zero so that the static parameter perturbation is the only input considered. Recall that $p_2 = p_1 + \Delta p$ and consider a periodic orbit of $\dot{x} = F(x, q + \beta\Delta p)$ where $|\beta| < 1$. The phase and isostable dynamics of θ^q and ψ_1^q resulting from this static parameter perturbation are

$$\begin{aligned}
\dot{\theta}^q &= \omega^q + \beta\Delta p Z^q(\theta^q) \cdot \frac{\partial F}{\partial p} + \mathcal{O}(\epsilon^2), \\
\dot{\psi}_1^q &= \kappa_1^q \psi_1^q + \beta\Delta p I_1^q(\theta^q) \cdot \frac{\partial F}{\partial p} + \mathcal{O}(\epsilon^2),
\end{aligned} \tag{60}$$

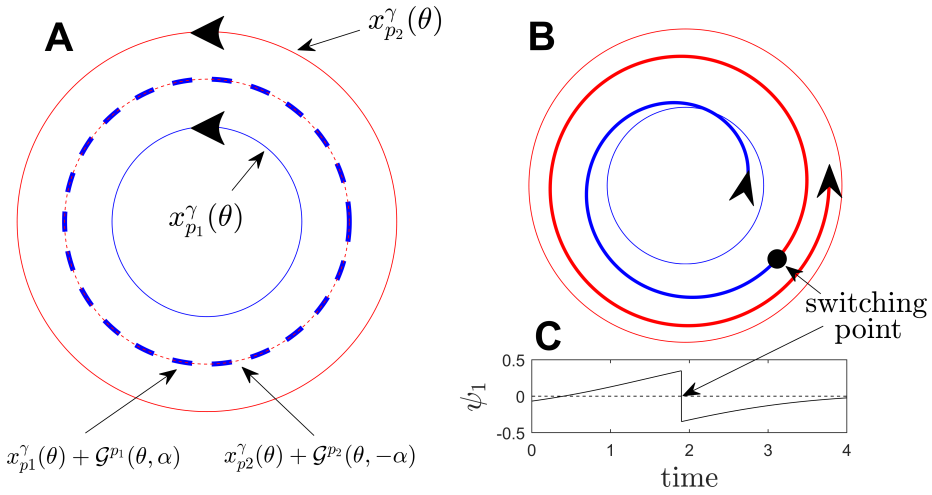

Figure 1: Panel A shows a representation of two periodic orbits of (57) in a two-dimensional cross section. $x^\gamma_{p_1}$ and $x^\gamma_{p_2}$ result when using parameters $p = p_1$ and $p = p_2$ in (57) and are shown as solid blue and red lines, respectively. Provided that p_1 and p_2 are close enough in magnitude, there will be some isostable coordinate $\alpha = \psi_1^{p_1} = -\psi_1^{p_2}$ at which the trajectories are close to each other. These points provide switching points that can be used to keep the isostable coordinates small, thereby limiting the magnitude of the amplitude coordinates and allowing for a more accurate reduction. This general idea is illustrated in panel B: a trajectory starts nearby the blue orbit and can represented by a phase-amplitude reduction (9) computed for the blue orbit. As the trajectory is perturbed towards the red orbit, the associated isostable coordinate starts to grow. At the switching point, the phase and isostable coordinates are recomputed in terms of a second reduction associated with the red orbit. As illustrated in panel C, this allows the isostable coordinates to remain small in magnitude resulting in a better characterization of the full system behavior. Multiple orbits can be stitched together in this fashion to analyze the overall system to implement a so-called patchwork reduction.

where $\partial F/\partial p$ is evaluated at $x^\gamma_q(\theta^q)$, and Z^q (resp., I_1^q) gives the gradient of the phase (resp., isostable) coordinate evaluated on the periodic orbit. It will be assumed that ψ_1^q is an $\mathcal{O}(\epsilon)$ term because Δp is $\mathcal{O}(\epsilon)$. Let $\phi^q \equiv \theta - (\omega^q - \beta\zeta\Delta p)t$ define a rotating reference frame where $\zeta \equiv \frac{1}{T^q}\int_0^{2\pi}\int_0^{T^q}\left[Z^q(s+\omega^q t)\cdot\frac{\partial F}{\partial p}\right]dtds$. Here $T^q = \omega^q/2\pi$ is the nominal period of oscillation for the periodic orbit when using $p = q$. Changing coordinates of (60) to work in this rotating reference frame and dropping $\mathcal{O}(\epsilon^2)$ terms yields

$$\begin{aligned}\dot{\phi}^q &= \beta\Delta p\left(-\zeta + Z^q(\phi^q + (\omega^q - \beta\zeta\Delta p)t)\cdot\frac{\partial F}{\partial p}\right),\\ \dot{\psi}_1^q &= \kappa_1^q\psi_1^q + \beta\Delta p I_1^q(\phi^q + (\omega^q - \beta\zeta\Delta p)t)\cdot\frac{\partial F}{\partial p}.\end{aligned} \tag{61}$$

Noticing that (61) is periodic in time, assuming that ψ_1^q is $\mathcal{O}(\epsilon)$, formal averaging techniques [47], [48] can be applied to approximate (61) as

$$\begin{aligned}\dot{\Phi}^q &= \beta\Delta p(W_\phi^q(\Phi^q) - \zeta),\\ \dot{\Psi}_1^q &= \kappa_1^q\Psi_1^q + \beta\Delta p W_\psi^q(\Phi^q),\end{aligned} \tag{62}$$

where $W_\phi^q(\Phi^q) = \frac{1}{T^{q,s}}\int_0^{T^{q,s}} \big(Z^q(\Phi^q + (\omega^q - \zeta\beta\Delta p)t)\cdot\frac{\partial F}{\partial p}\big)dt$, and $W_\psi^q(\Phi^q) = \frac{1}{T^{q,s}}\int_0^{T^{q,s}} \big(I_1^q(\Phi^q + (\omega^q - \zeta\beta\Delta p)t)\cdot\frac{\partial F}{\partial p}\big)dt$, with $T^{q,s} = 2\pi/(\omega^q - \zeta\beta\Delta p)$. Using a change of variables $t^* = (\omega^q - \zeta\beta\Delta p)/\omega^q$, one can show that $W_\phi^q(\Phi^q) = \frac{1}{T^q}\int_0^{T^q} \big(Z^q(\Phi^q + \omega^q t^*)\cdot\frac{\partial F}{\partial p}\big)dt^*$ and $W_\psi^q(\Phi^q) = \frac{1}{T^q}\int_0^{T^q} \big(I_1^q(\Phi^q + \omega^q t^*)\cdot\frac{\partial F}{\partial p}\big)dt^*$, and are not dependent on Δp. As explained in [47], fixed points of (62) correspond to periodic orbits of (61) with the same stability. Noting that ζ is the average of $W_\phi^q(\Phi^q)$ and that $W_\phi^q(\Phi^q)$ is periodic, provided W_ϕ^q is not constant there must be some value Φ_{fp}^q for which $W_\phi^q(\Phi_{\text{fp}}^q) - \zeta = 0$ and $W'^q_\phi(\Phi_{\text{fp}}^q) < 0$, where $' \equiv d/d\Phi^q$. With this value of Φ_{fp}^q, the bottom equation of (62) has a stable fixed point at

$$\Psi_{\text{fp}}^q = -\frac{\beta\Delta p W_\psi^q(\Phi_{\text{fp}}^q)}{\kappa_1^q}. \tag{63}$$

In light of (63), consider the periodic orbit $x_{p_1}^\gamma$ with a static parameter change $\beta\Delta p$. Additionally, consider the periodic orbit $x_{p_2}^\gamma$ with a static parameter change $(\beta-1)\Delta p$. Using (63), one can show that $\Psi_{\text{fp}}^{p_1} = -\Psi_{\text{fp}}^{p_2}$ when

$$\beta = \frac{W_\psi^{p_2}(\Phi_{\text{fp}}^{p_2})\kappa_1^{p_1}}{W_\psi^{p_2}(\Phi_{\text{fp}}^{p_2})\kappa_1^{p_1} - W_\psi^{p_1}(\Phi_{\text{fp}}^{p_1})\kappa_1^{p_2}}. \tag{64}$$

Note that (62) approximates the behavior of (61), and that the output of (61) can be used in turn to approximate the state using (59). Additionally, because the limiting behavior of both orbits approximates the stable periodic orbit using $p = p_1 + \beta\Delta p$, one finds that

$$x_{p_1}^\gamma(\theta^{p_1}) + \mathcal{G}^{p_1}(\theta^{p_1}, \Psi_{\text{fp}}^{p_1}) \approx x_{p_2}^\gamma(\theta^{p_2}) + \mathcal{G}^{p_2}(\theta^{p_2}, -\Psi_{\text{fp}}^{p_1}). \tag{65}$$

4.2 Converting Phase and Isostable Coordinates Between Orbits

Equation (65) illustrates that the outputs using two nearby periodic orbits overlap at predictable isostable coordinates. This knowledge can be used to switch between the phase and isostable coordinates as necessary in order to keep isostable coordinates low thereby resulting in an accurate representation of the output behavior in situations where a single periodic orbit is insufficient. In order to switch between orbits, it is necessary to relate the phase and isostable coordinates of adjacent orbits. Toward this end, first consider a hypersurface $x_{p_2}^\gamma(\theta^{p_2}) + \mathcal{G}^{p_2}(\theta^{p_2}, \psi_1^{p_2})$. Let $x_0 = \begin{bmatrix} x_1 & \dots & x_N \end{bmatrix}^T$ be any initial condition on this hypersurface with corresponding phase and isostable coordinates θ and $\psi_1^{p_2}$ (with $\psi_j^{p_2} = 0$ for $j \geq 2$). Using Taylor expansion, any small perturbation Δx from this initial condition can be represented to leading order according to

$$\Delta x = A_\Psi^{p_2}\Delta\Psi^{p_2}, \tag{66}$$

where $\Delta\Psi^{p_2} \equiv \begin{bmatrix}\Delta\theta & \Delta\psi_1 & \dots & \Delta\psi_{N-1}\end{bmatrix}^T$ and

$$A_\Psi^{p_2} \equiv \begin{bmatrix}\big(\frac{\partial x_{p_2}^\gamma}{\partial\theta} + \frac{\partial\mathcal{G}^{p_2}}{\partial\theta}\big) & \frac{\partial\mathcal{G}^{p_2}}{\partial\psi_1} & g^2(\theta^{p_2}) & \dots & g^{N-1}(\theta^{p_2})\end{bmatrix}, \tag{67}$$

with all partial derivatives evaluated at θ^{p_2} and $\psi_1^{p_2}$. Note that the terms $g^2, \dots, g^{N-1}$ corresponding to perturbations to the isostable coordinates $\psi_2^{p_2}, \dots, \psi_{N-1}^{p_2}$ are not considered in the reduction (9), however, they are necessary to allow for perturbations in any direction from x_0. Finally, provided $A_\Psi^{p_2}$ is invertible, the change in phase and isostable coordinates is given by

$$\Delta\Psi = \big(A_\Psi^{p_2}\big)^{-1}\Delta x. \tag{68}$$

From (53), when $\psi_1^{p_2} = 0$, $A_\Psi^{p_2}$ is always invertible, with

$$\left(A_\Psi^{p_2}\big|_{\psi_1^{p_2}=0}\right)^{-1} = \begin{bmatrix} Z_1(\theta) & I_1(\theta) & \dots & I_{N-1}(\theta) \end{bmatrix}^T, \tag{69}$$

where $Z_1, I_1, \dots, I_{N-1}$ are the phase and isostable response curves for the periodic orbit $x_{p_2}^\gamma(\theta)$. Provided $\psi_1^{p_2}$ is small enough, $A_\Psi^{p_2}$ will also be invertible.

Equation (68) can be used to convert coordinates between periodic orbits. To do so, suppose that

$$x_{p_1}^\gamma(\theta^{p_1}) + \mathcal{G}^{p_1}(\theta^{p_1}, \psi_1^{p_1}) \approx x_{p_2}^\gamma(\theta^{p_2}) + \mathcal{G}^{p_2}(\theta^{p_2}, \psi_1^{p_2}), \tag{70}$$

with $-\psi_1^{p1} \approx \psi_1^{p_2}$. Noting that location on the periodic orbit corresponding to $\theta^{p_1} = 0$ and $\theta^{p_2} = 0$ is arbitrary, it will be assumed that these orbits have been appropriately aligned so that $\theta^{p_1} \approx \theta^{p_2}$. A more detailed discussion of this required alignment is given in Appendix B. Equality in (70) can be obtained by allowing for a perturbation to the isostable coordinates with respect to the orbit $x_{p_2}^\gamma$,

$$x_{p_1}^\gamma(\theta^{p_1}) + \mathcal{G}^{p_1}(\theta^{p_1}, \psi_1^{p_1}) = x_{p_2}^\gamma(\theta^{p_1}) + \mathcal{G}^{p_2}(\theta^{p_1}, -\psi_1^{p_1}) + A_\Psi^{p_2}\Delta\Psi, \tag{71}$$

where $A_\Psi^{p_2}$ is evaluated at $\psi_1^{p_2} = -\psi_1^{p_1}$ and $\theta^{p_2} = \theta^{p_1}$. By solving

$$\Delta\Psi = \left(A_\Psi^{p_2}\right)^{-1}\left[x_{p_1}^\gamma(\theta^{p_1}) + \mathcal{G}^{p_1}(\theta^{p_1}, \psi_1^{p_1}) - x_{p_2}^\gamma(\theta^{p_1}) - \mathcal{G}^{p_2}(\theta^{p_1}, -\psi_1^{p_1})\right], \tag{72}$$

one finds that the converted phase and isostable coordinates are

$$\begin{aligned} \theta^{p_2} &= \theta^{p_1} + \Delta\theta, \\ \psi_1^{p_2} &= -\psi_1^{p_1} + \Delta\psi_1. \end{aligned} \tag{73}$$

As a final note, because $\Delta\psi_2, \dots, \Delta\psi_{N-1}$ are not explicitly required, the terms $g^2(\theta), \dots, g^{N-1}(\theta)$ do not need to be computed. Instead, one can replace the columns $g^2(\theta^{p_2}), \dots, g^{N-1}(\theta^{p_2})$ from (67) with a set of vectors spanning the orthogonal complement of the set $\{Z_1(\theta), I_1(\theta)\}$, where the phase and isostable response curves are associated with the periodic orbit $x_{p_2}^\gamma$. Solving for $\Delta\Psi$ using this modified version of $A_\Psi^{p_2}$ will have no influence on the values of $\Delta\theta$ and $\Delta\psi_1$ and eliminates the need to compute $g^2(\theta^{p_2}), \dots, g^{N-1}(\theta^{p_2})$. Justification for this is given at the end of Section 3.2.3.

5 Examples and Illustrations of the High-Order Reduction Strategy

High-Accuracy Phase-amplitude Reduction of the Nonradial Isochron Clock

Here the high-accuracy phase-amplitude reduction strategy described in previous sections is applied to the non-radial isochron clock

$$\begin{aligned} \dot{x}/P &= \sigma x(1 - (x^2 + y^2)^{1/2}) - y(1 + \rho((x^2 + y^2)^{1/2} - 1)) + u(t), \\ \dot{y}/P &= \sigma y(1 - (x^2 + y^2)^{1/2}) + x(1 + \rho((x^2 + y^2)^{1/2} - 1)), \end{aligned} \tag{74}$$

which has been modified from the radial isochron clock given in [1] to include a radial dependence on the rate of rotation. Here, $u(t)$ is an external perturbation and parameters P, σ, and ρ are taken to be 1, 0.08, and 0.12, respectively. For this choice of parameters, when $u(t) = 0$ the system settles to a periodic orbit $[x(t), y(t)] = [\cos(2\pi t), \sin(2\pi t)]$ with a Floquet exponent $\kappa_1 = -1.005$ and corresponding Floquet multiplier $\lambda_1 = 0.366$. Because (74) is planar, the phase-amplitude

equations (9) do not reduce the dimensionality of the reduction (more complicated equations will be considered in subsequent examples).

Towards computation of the necessary terms of the phase-amplitude reduction (9), Δx from (10) is taken to fourteenth order accuracy in the isostable coordinate. The powers of the isostable coordinates from (15) and (12) are matched to find relations of the form (18) that are used to calculate the necessary terms of the expansion (10). Likewise, the powers of the isostable coordinates in the expansions (30) (resp., (40)) are matched to find relations of the form (34) (resp., (44)) that are used to compute the necessary terms of the expansions in (22). This process of matching terms to identify the relations from (18), (34), and (44) is performed with a symbolic computational package. The resulting equations are solved using strategies detailed in Section 3. Panel A of Figure 2 shows a surface plot of the $\mathcal{Z}_x(\theta,\psi_1) \equiv \frac{\partial \theta}{\partial x}$ and $\mathcal{I}_{1,x}(\theta,\psi_1) \equiv \frac{\partial \psi_1}{\partial x}$ calculated to different orders of accuracy in the isostable coordinate. The leftmost plots give zeroth order approximations, which are simply sinusoids that have no dependence on the amplitude coordinate. A much richer description of the perturbed response results when higher order accuracy approximations are computed. The reduction (9) can be used to give an approximation of the isochrons of the system as defined in (2). This is accomplished by computing the terms of $\mathcal{G}(\theta,\psi_1)$ to desired accuracy and plotting the level sets of the phase. Panel B shows the estimate of the isochrons as colored lines obtained by taking the $\mathcal{G}(\theta,\psi_1)$ to first, sixth, and fourteenth order. Black lines show the true isochrons computed directly from (2). The first order approximation estimates the isochrons to be straight lines, with true values of the isochrons that diverge rapidly at larger distances from the periodic orbit. Approximating $\mathcal{G}(\theta,\psi_1)$ to higher orders of accuracy in ψ_1 provides an increasingly accurate estimate of the curvature of the isochrons.

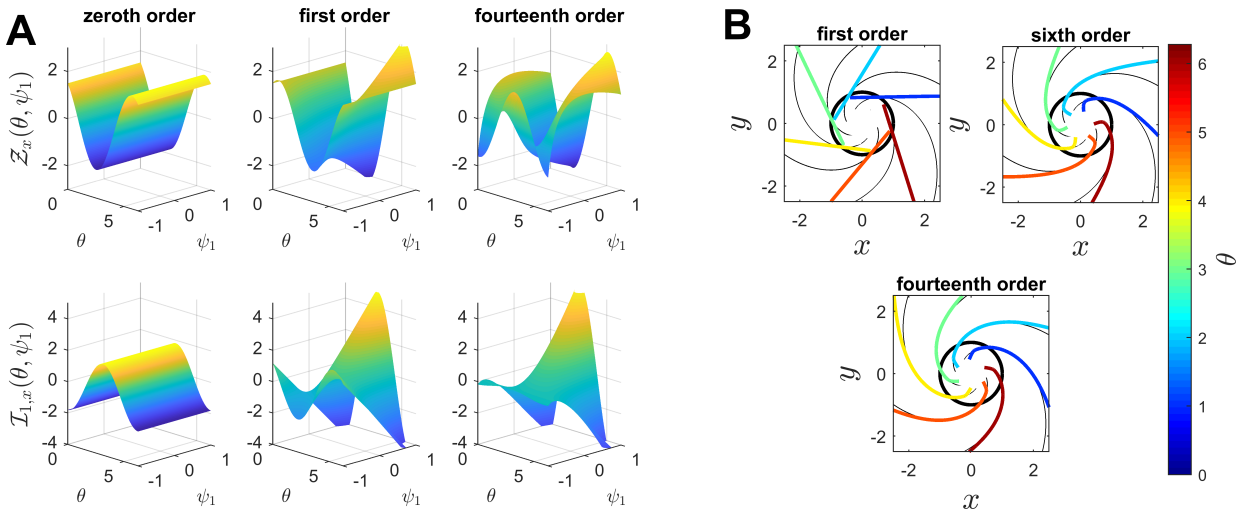

Figure 2: Panel A shows approximations of $\frac{\partial \theta}{\partial x}$ and $\frac{\partial \psi_1}{\partial x}$ that are valid up to fourteenth order in ψ_1. Increasing the order of accuracy provides a richer picture of the perturbed response. Panel B shows approximations of the isochrons obtained by computing $G(\theta,\psi_1)$ to various orders of accuracy. Black lines show the true isochrons for the nonradial isochron clock (74) computed directly from the definition (2).

The forced response of the phase-amplitude representation of the nonradial isochron clock (74) is also investigated with various types of perturbations. Representative results are shown in Figure 3. Panel A shows the output resulting from a pulse $u(t) = 25$ applied for 0.1 time units starting from

the periodic orbit. Note that the second order reduction initially overshoots the response worse than the zeroth order reduction; the large inputs considered here take the lower order reductions far beyond their regions of applicability making the reduced model behavior unpredictable. Panel C shows the limiting behavior in response to a sinusoidal input $u(t) = 25\sin(2\pi t/1.6)$. In each panel, the solid black line shows the response from the full equations (74) and colored lines show the output from the phase-amplitude representation (9) computed to various orders of accuracy in ψ_1. Here, an order k accuracy reduction takes both $\mathcal{Z}$ and $\mathcal{I}_1$ to k^{th} order accuracy in ψ_1 and $\mathcal{G}$ to $k+1^{\text{th}}$ order accuracy. This convention is adopted so that the 0^{th} order accuracy reduction corresponds to a standard phase and isostable reduction in concert with a standard implementation of Floquet theory. Panels B and D correspond the error between the full model simulations where $X(t) = \begin{bmatrix} x(t) & y(t) \end{bmatrix}^T$ for the full model simulations and $X^*(t)$ gives the corresponding output from the phase-amplitude equations.

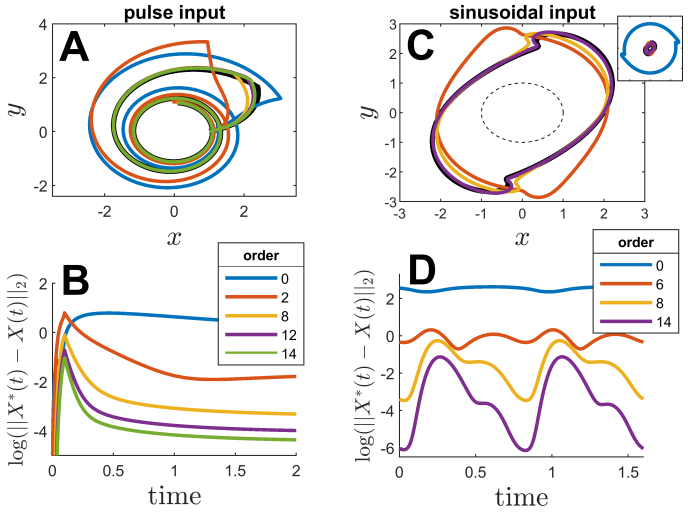

Figure 3: Panels A shows the transient behavior of the phase-amplitude reduction (colored lines) and the full model equations of the non-radial isochron clock (black line) in response to a short pulse. Likewise, panel C shows the limiting behavior in response to a large magnitude sinusoidal perturbation with the dashed black line showing the unperturbed periodic orbit for reference. The top-right axis in panel C highlights the order zero reduced response in relation to the other curves. Panel B (resp., D) show the resulting error between the phase-amplitude reduction and the full equations from panels A (resp., C) when using the reduction of the indicated order of accuracy.

In each trial from Figure 3, the overall error between the phase-amplitude reduced equations and the full model equations decreases predictably as the order of accuracy is increased. At fourteenth order accuracy, there is little discernible error between the phase-amplitude reduced equations and the full model simulations. When using the sinusoidal input, the order 1 through 5 reductions do not converge to a periodic solution and instead become unbounded as time increases (not shown). While the 0^{th} order phase-amplitude equations do converge to a periodic solution, there is a large amount of error as illustrated in the upper-right corner of panel C where axis has been rescaled to fit the resulting orbit; the order 0 phase-amplitude reduction is useless for the magnitude of perturbations considered in the example.

Patchwork Reduction Illustrated in a Model for Circadian Oscillations

In this example, a model with relevance to circadian rhythms will be considered and the high-order phase-amplitude patchwork reduction strategy will be employed to examine a control strategy for mitigation of circadian misalignment. Over the course of many millennia, organisms have developed highly tuned circadian rhythms to anticipate and respond to to predictable changes in their 24-hour environment [49]. The free-running circadian cycles of most organisms are close to 24 hours so that they can be stably entrained to a 24-hour light-dark cycle [50], [51]. Circadian misalignment is represents a disruption to this steady entrainment; when the disruption is caused by rapid transcontinental travel it is referred to as jet-lag [52], [53].

Recently there has been a growing interest in understanding dynamical mechanisms governing jet-lag [54], [20], [55], [29] in order to develop control strategies to limit its negative effects, [56], [57], [58]. Phase reduction has often been used as a preliminary step in analyzing the underlying dynamics of complicated oscillatory models, but as [20] points out, phase reduction (and phase-amplitude reduction methods in general) are difficult to implement because the exogenous 24-hour light cycle perturbations are usually large enough in magnitude to drive the system far from its underlying limit cycle thereby rendering the reduction invalid. Consequently, it has been difficult to utilize phase reduction methods in the development control strategies for jet-lag mitigation. Here, the high-accuracy phase-amplitude reduction and the patchwork reduction strategy will be applied to a circadian model to illustrate its utility as a reduction framework in the aforementioned setting. The specific model characterizes gene regulation [59] and has been used to model the mammalian circadian cycle:

$$\begin{aligned}
\dot{B} &= v_1 \frac{K_1^n}{K_1^n + D^n} - v_2 \frac{B}{K_2 + B} + L_c + L(t_s) + \Delta L(t), \\
\dot{C} &= k_3 B - v_4 \frac{C}{K_4 + C}, \\
\dot{D} &= k_5 C - v_6 \frac{D}{K_6 + D}.
\end{aligned} \tag{75}$$

Here, B, C, and D, are used to represent concentrations of mRNA of the clock gene, associated protein, and nuclear form of the protein, respectively. $L(t_s)$ incorporates the influence of an external, 24-hour light-dark cycle taken to be

$$L(t_s) = L_0 \left[\frac{1}{1 + \exp(-5(t_s - 6))} - \frac{1}{1 + \exp(-5(t_s - 18))} \right],$$

where L_0 is the nominal maximum intensity of light, $t_s = \text{mod}(t, 24)$, and sigmoidal functions are incorporated so that the light intensity changes smoothly between its maximum and minimum values, and $\Delta L(t)$ will be used to implement a light exposure or avoidance strategy in order to hasten recovery from circadian misalignment. Above, L_c is treated as a variable parameter to implement the patchwork reduction strategy from Section 4. Nominally $L_c = 0$, but can be modified when using the patchwork reduction to produce different periodic orbits. From this perspective, $U(t)$ from (57) is $\begin{bmatrix}(L(t_s) + \Delta L(t)) & 0 & 0\end{bmatrix}^T$. When using the patchwork reduction, $U_p(t) = \begin{bmatrix}(L(t_s) + \Delta L(t) - L_c) & 0 & 0\end{bmatrix}^T$. For the model equations from (75), parameters are taken to be $n = 6, v_1 = 0.84, v_2 = 0.42, v_4 = 0.35, v_6 = 0.35, K_1 = 1, K_2 = 1, K_4 = 1, K_6 = 1, k_3 = 0.7$, and $k_5 = 0.7$. Minor changes in parameters are made compared to those given in Figure 1 of [59] so that in the absence of light (i.e., when $L_0 = L_c = 0$) the model has a stable limit cycle with period 24.2 hours.

For the moment, (75) will be analyzed taking $\Delta L(t) = 0$. The resulting limit cycle is analyzed using the high-accuracy phase-amplitude reduction framework with results shown in Figure 4. Panel A shows $B(t)$ plotted for the resulting limit cycle taking $L_0 = L_c = 0$. The orbit has two Floquet multipliers—one with $\lambda_1 = 0.37$ with corresponding Floquet exponent $\kappa_1 = -0.041$ and the other being close to zero so that it can be ignored in the reduction. The blue curve in panel B shows a three dimensional representation of this orbit as a solid blue line. Additionally, the black lines in Figure show a subset of the 64 orbits that will be used to implement the patchwork reduction obtained by taking $L_0 = 0$ and $L_c \in [-0.0051, 0.0138]$. Note that $L_c < 0$ implies the application of negative light, which is not possible in a physical sense, but does result in periodic orbits in (75). Panel C of Figure 4 shows surface plots of $\mathcal{Z}_B(\theta, \psi_1) \equiv \frac{\partial \theta}{\partial B}$ and $\mathcal{I}_{1,B}(\theta, \psi_1) \equiv \frac{\partial \psi_1}{\partial B}$ for the blue curve from panel B (i.e., the limit cycle obtained for $L_0 = L_c = 0$) calculated to various orders of accuracy in ψ_1 using the methods described in Section 3.2. Higher order approximations of $\mathcal{Z}_B$ and $\mathcal{I}_{1,B}$ provide increasingly accurate representations of the perturbed dynamical behavior which is reflected in the overall accuracy of (9) in the examples to follow.

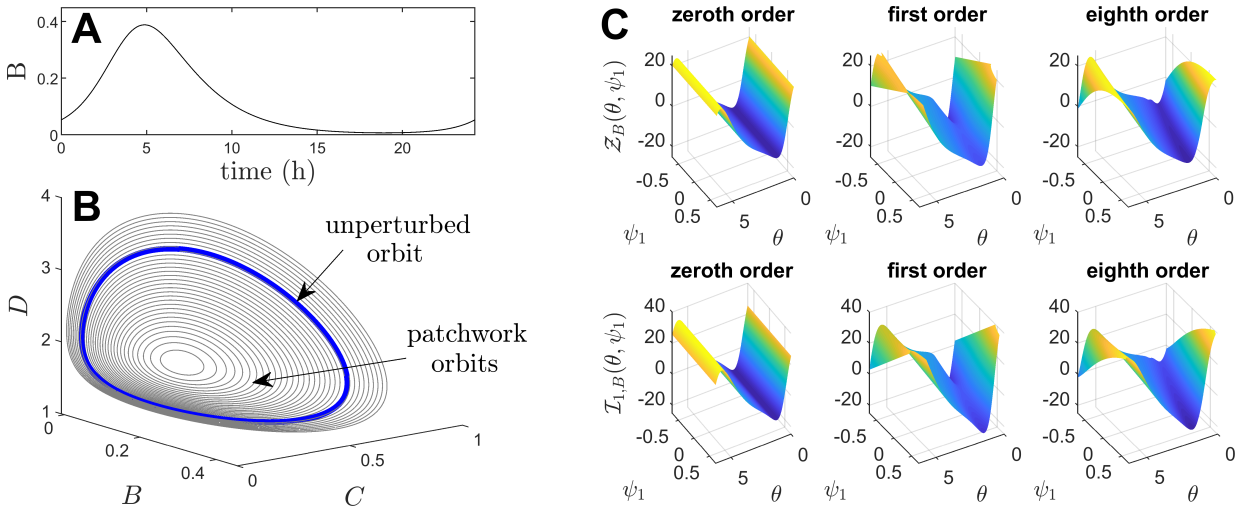

Figure 4: Panel A shows a trace of $B(t)$ from the resulting limit cycle of (75) when taking $L(t) = \Delta L(t) = L_c = 0$. The blue line in panel B shows the same periodic orbit along with a family of periodic orbits (in black) that result when taking $L(t_s) = \Delta L(t) = 0$ and varying L_c. These orbits are used to implement the patchwork reduction strategy. Surface plots in panel C show reduced functions from (9) to different orders of accuracy in ψ_1.

The reduced functions $\mathcal{Z}_B$ and $\mathcal{I}_{1,B}$ shown in Figure 4 are obtained by first computing Δx from (10) to the desired order of accuracy in ψ_1 using equations of the form (18). Subsequently, the phase and isostable gradients are calculated to the desired order of accuracy using equations of the form (34) and (44). As explained in Section 3.2.3, it is possible to calculate $\mathcal{Z}_B$ and $\mathcal{I}_{1,B}$ directly from the expansion of Δx. Panels A and B of Figure 5 compare the eighth order response functions $\mathcal{Z}_B(\theta, \psi_1)$ and $\mathcal{I}_{1,B}(\theta, \psi_1)$ (as shown in Panel C of Figure 4) to the inferred curves $\mathcal{Z}_B^{\text{inferred}}(\theta, \psi_1)$ and $\mathcal{I}_{1,B}^{\text{inferred}}(\theta, \psi_1)$ as computed from (52) using the eighth order accurate expansion of $\mathcal{G}(\theta, \psi_1)$. Because $\mathcal{Z}_B(\theta, \psi_1)$ and $\mathcal{I}_{1,B}(\theta, \psi_1)$ are computed directly for the asymptotic expansions (22) they are taken to be the ground truth for the system. Correspondingly, $\mathcal{Z}_B(\theta, \psi_1) - \mathcal{Z}_B^{\text{inferred}}(\theta, \psi_1)$ and $\mathcal{I}_{1,B}(\theta, \psi_1) - \mathcal{I}_{1,B}^{\text{inferred}}(\theta, \psi_1)$ give the error when using (52). As predicted from the asymptotic expansion of $(A_\Psi)^{-1}$ from (56), for a given value of θ the accuracy of $\mathcal{Z}_B^{\text{inferred}}(\theta, \psi_1)$ and $\mathcal{I}_{1,B}^{\text{inferred}}(\theta, \psi_1)$ depends

strongly on the condition number of $A_\Psi|_{\psi_1=0}$ shown in panel C, with larger condition numbers leading to larger errors.

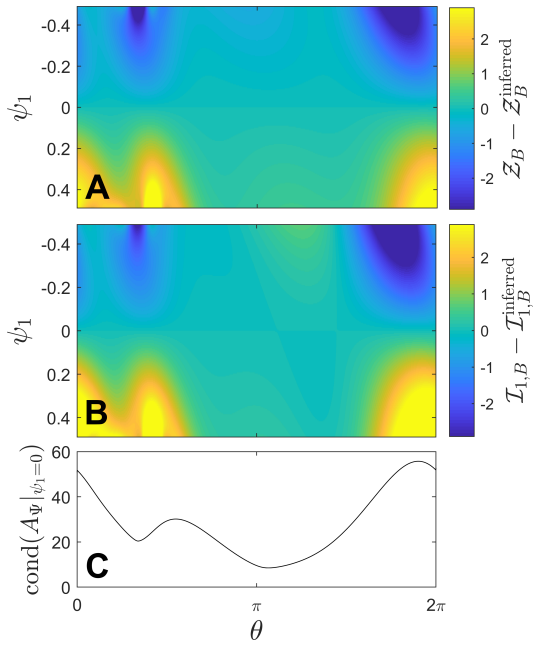

Figure 5: Panel A (resp., B) gives a comparison of $\mathcal{Z}_B(\theta,\psi_1)$ (resp., $\mathcal{I}_{1,B}(\theta,\psi_1)$) computed using methods from Section 3.2 versus $\mathcal{Z}_B(\theta,\psi_1)^{\text{inferred}}$ (resp., $\mathcal{I}_{1,B}^{\text{inferred}}(\theta,\psi_1)$) which are calculated from (52). Panel C illustrates that for a given value of θ the error resulting in the inferred functions grows with the condition number of $A_\Psi|_{\psi_1=0}$.

In order to implement the patchwork phase-amplitude reduction as described in Section 4, $\mathcal{G}(\theta,\psi_1)$, $\mathcal{Z}(\theta,\psi_1)$, and $\mathcal{I}_1(\theta,\psi_1)$ are computed for 64 limit cycles that result when taking $L_0 = 0$ and $L_c \in [-0.0051, 0.0138]$. In simulations of the patchwork reduction, the state is initially assigned a nominal periodic orbit $x^\gamma_{L_c}(\theta)$ where the subscript L_c indicates the value of light used to obtain the orbit. The reduced equations (9) are simulated using the $\mathcal{G}(\theta,\psi_1)$, $\mathcal{Z}(\theta,\psi_1)$, and $\mathcal{I}_1(\theta,\psi_1)$ that correspond to the nominal orbit $x^\gamma_{L_c}(\theta)$ taken to third order accuracy in ψ_1. At every timestep in the simulation, $\Delta\psi_1$ and $\Delta\theta$ from (73) are computed using adjacent periodic orbits $x^\gamma_{L_c-\Delta L_c}(\theta)$ and $x^\gamma_{L_c+\Delta L_c}(\theta)$. If the following conditions:

$$\begin{aligned} |-\psi_1 + \Delta\psi_1| &< |\psi_1|, \\ |\Delta\psi_1| &< 0.15, \\ |\Delta\theta| &< 0.05, \end{aligned} \tag{76}$$

are all satisfied for either of the adjacent orbits, the state is updated according to $\theta^{\text{update}} = \theta + \Delta\theta$ and $\psi_1^{\text{update}} = -\psi_1 + \Delta\psi_1$ and the nominal orbit is also updated accordingly. Switching between orbits in this manner allows the value of the isostable coordinate to remain small even when using large values for L_0.

Figure 6 shows the results of simulations of (75) for various magnitudes of L_0 in the 24-hour light-dark cycle. Three different reductions are used. The first uses the eighth order accurate version of (9). The second implements the patchwork reduction strategy described above taking $\mathcal{Z}, \mathcal{I}_1$, and $\mathcal{G}$ to third order accuracy in ψ_1 for each orbit. The third uses a standard implementation of phase

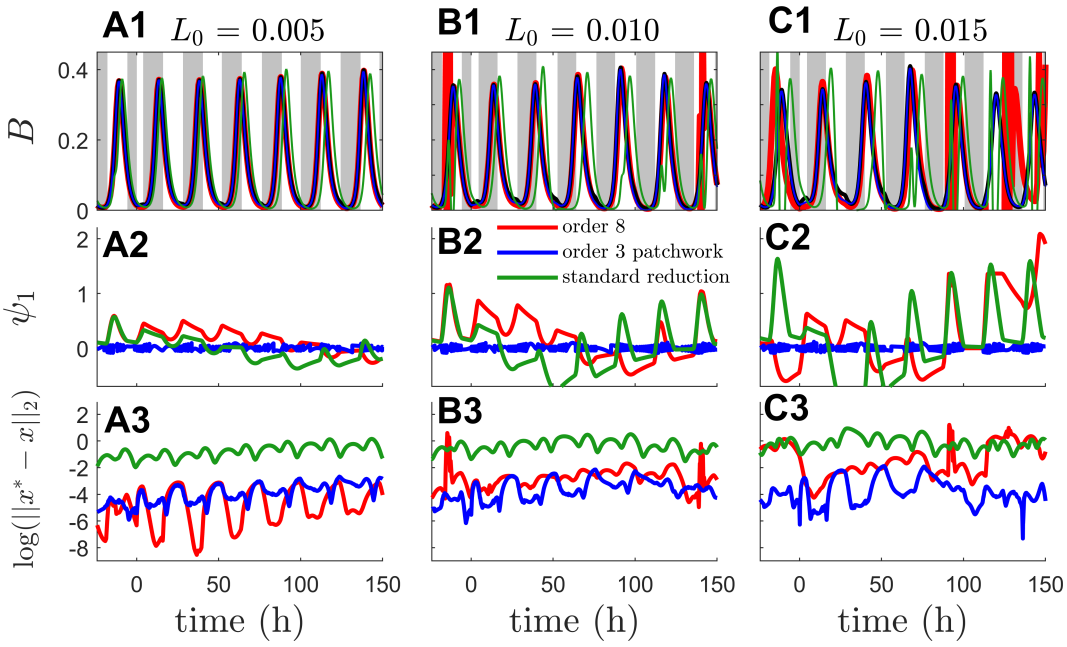

Figure 6: Reentrainment of the circadian model (75) after a -10 hour time shift occuring at $t = 0$ hours. The output of three different reduced order models for different values of external light intensity (L_0) is shown in panels A1, B1, and C1. Colored lines correspond to the indicated reduced model and the black line gives the output from full model simulations. Alternating black and grey lines correspond to the light-dark cycle, with grey corresponding to times for which $L(t_s) < L_0/2$ (i.e., night time). Note that the order 8 reduction (red line) completely breaks down for $L_0 = 0.010$ and $L_0 = 0.015$ at times when $\psi_1 > 1$. Panels A2, B2, and C2 show corresponding isostable coordinates during each simulation and panels A3, B3, and C3 show the error between the reduced model outputs and the full model simulations. The patchwork reduction is the only viable reduced model for $L_0 > 0.010$.

reduction (i.e., with $\mathcal{Z}$, $\mathcal{I}_1$, and $\mathcal{G}$ computed to zeroth, zeroth, and first order in ψ_1, respectively). The terms of the non-patchwork phase-amplitude reductions are obtained using the limit cycle that results from taking $L_c = 0$. Panels A, B, and C of Figure 6 illustrate results for $L_0 = 0.005, 0.010$, and 0.015, respectively. In each simulation from Figure 6, the external light $L(t_s)$ is applied long enough so that initial transients die out and the circadian cycle is fully entrained. At $t = 0$, the external time t_s is suddenly shifted by -10 hours, simulating rapid westward travel through 10 time zones and the subsequent reentrainment is illustrated in panels A1, B1, and C1. Panels A2, B2, and C2 illustrate the isostable coordinate ψ_1 over the course of simulations and panels A3, B3, and C3 show the error between solutions of the full equation and reduced equations where $x(t) = \begin{bmatrix} B(t) & C(t) & D(t) \end{bmatrix}^T$ for the full model (75), and $x^*(t)$ is the corresponding output from the phase-amplitude reduction. In all simulations shown below, the reentrainment time is defined as the amount of time required for the phase to return to within one hour of its steady state behavior. In these simulations $L_0 = 0.005$ is a relatively small value for the magnitude of external light and the unreduced model takes 208 hours before reentrainment occurs after the -10 hour time shift. Despite this, the standard reduction does not accurately characterize the output during reentrainment, with errors $||x^* - x||_2$ that are always on the order of $\exp(-1)$. For $L_0 = 0.005$, the eighth order accurate reduction outperforms the patchwork reduction. As the value of L_0 increases, the patchwork

reduction begins to significantly outperform all of the other reductions. By allowing for the nominal orbit to switch as that simulation progresses, the isostable coordinates remain low resulting in an accurate representation of the model output. For $|\psi_1| \approx 1$ when using the eighth order accurate, non-patchwork reduction, the accuracy begins to degrade. It is worth noting that the eighth order accurate non-patchwork reduction only works for $L_0 = 0.005$ when using negative time shifts. Under the application of these perturbations the isostable coordinate tends to decrease during reentrainment. For positive time shifts corresponding to eastward travel (not shown), the isostable coordinate tends to increase ruining the applicability of the resulting reduction. Conversely, the patchwork phase-amplitude reduction accurately characterizes the output for any time shift for the values of L_0 considered here. For this reason, the patchwork phase-amplitude reduction will be used exclusively for the remainder of this example.

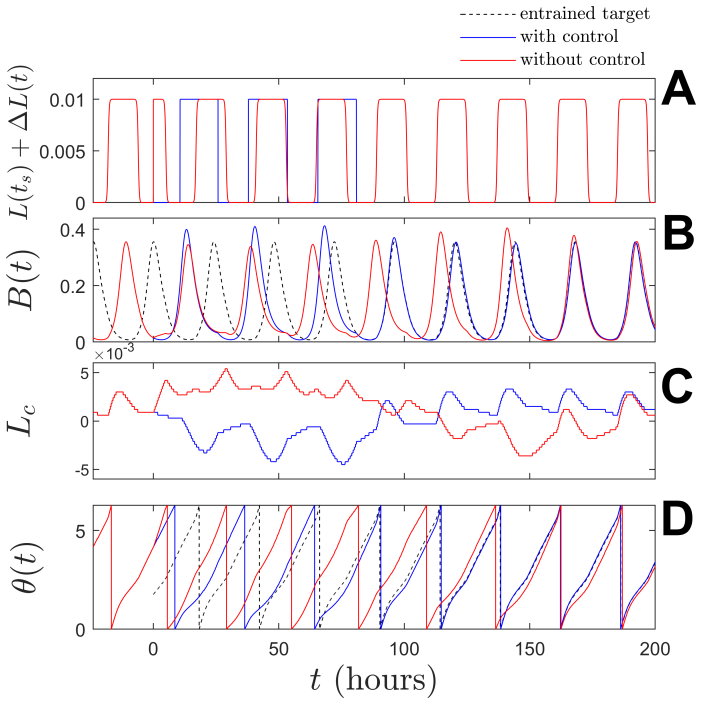

Figure 7: Reentrainment after a sudden shift in the day-light cycle. The full model (75) is simulated until it is fully entrained to $L(t_s)$. At $t = 0$, t_s is shifted by -11 hours. The patchwork phase-amplitude reduction is used to determine the control from (77) to hasten reentrainment. The resulting control is shown in Panel A (blue line) and compared to the nominal light-dark cycle in the uncontrolled case (red line). This control is applied to the full model with results shown in panel B. Panel C shows the nominal orbit during simulations of the patchwork phase-amplitude reduction, and panel D shows the phase during the controlled and uncontrolled recovery.

Finally, to demonstrate the utility of the patchwork reduction, a simple control strategy is implemented to speed reentrainment after large shifts in t_s. First, for a given value of L_0, the patchwork phase-amplitude reduction is simulated long enough for all transients die out. This fully entrained solution is taken to define $\theta^e(t_s)$ and $L_c^e(t_s)$ which gives the phase and nominal limit cycle

for the entrained solution. The following control strategy is implemented:

$$L(t_s)+\Delta L(t)=\begin{cases}0, & \text{if } \theta-\theta_{\text{targ}}>0 \text{ and } \mathcal{Z}(\theta,\psi_1)>0,\\ L_0, & \text{if } \theta-\theta_{\text{targ}}>0 \text{ and } \mathcal{Z}(\theta,\psi_1)\le 0,\\ L_0, & \text{if } \theta-\theta_{\text{targ}}<0 \text{ and } \mathcal{Z}(\theta,\psi_1)>0,\\ 0, & \text{if } \theta-\theta_{\text{targ}}<0 \text{ and } \mathcal{Z}(\theta,\psi_1)\le 0,\end{cases} \tag{77}$$

where, $\theta_{\text{targ}}=\theta^{\text{e}}(t_s)-\theta_s(L_c^{\text{e}}(t_s),L_c(t))$. Intuitively, the control strategy implements a light exposure or avoidance strategy that always seeks to move the phase coordinate towards towards the nominal entrained solution. For instance, if $\theta-\theta_{\text{targ}}>0$, the current phase is ahead of its target and the oscillation needs to be delayed. If $Z(\theta,\psi_1)$ is also positive, then a positive value of $L(t_s)+\Delta L(t)$ will advance the phase. As prescribed by (77), under these conditions $L(t_s)+\Delta L(t)$ will be set to zero (the lowest possible value) so that the phase advances as slowly as possible. As explained in Appendix B, the additional term $\theta_s(L_c^{\text{e}}(t_s),L_c(t))$ from θ_{targ} provides a small correction to account for the possibility that the nominal orbit $L_c^e(t_s)$ on the entrained target solution may be temporally misaligned with the nominal limit cycle $L_c(t)$ during the application of the control strategy.

Figure 7 shows results from using the control strategy (77) to recover from a sudden time shift. In these simulations, $L_0=0.010$. The model is initially fully entrained to $L(t_s)$ and at $t=0$, t_s is shifted by -11 hours. The control is calculated for the patchwork phase-amplitude model and shown in panel A (blue line). Once $|\theta-\theta_{\text{targ}}|<2\pi/24\approx 0.26$, which corresponds to a one hour difference from the solution that is fully entrained to the shifted $L(t_s)$, the control is turned off so that only $L(t_s)$ remains. The light applied in the uncontrolled case is shown in red. The resulting control is applied to the full equations (75) with the output shown in blue in panel B of Figure 7. The uncontrolled recovery is shown by the red curve and the fully entrained reference is given by a dashed line. Reentrainment occurs at 81.8 hours after the initial shift in time when the control strategy (77) is implemented. Without control reentrainment takes 161.2 hours. Panel C shows the nominal orbit used during the patchwork phase-amplitude reduction strategy as a function of time. Note that while $L_c<0$ during the application of the control strategy, negative light is never actually applied by (77). Rather, a negative value of L_c indicates that the trajectory has made a close approach to a periodic orbit that would result from taking $L_c<0$. Finally, panel D shows the phase with and without control compared to the entrained target trajectory. Recovery from other time shifts is improved most by the control strategy when the time shifts are large. For shifts that advance time between 10 and 17 hours, the control strategy (77) reduces the recovery time by at least 15 percent with the largest improvements in recovery time resulting from time shifts near 13 hours (-11 hours).

Because the control strategy implemented in (77) is merely a local strategy that attempts to reduce $\theta-\theta_{\text{targ}}$ at every instant, one would expect that a more sophisticated control strategy that attempts to minimize some global measure of recovery time would perform better. There is an additional challenge associated with the implementation of optimal control strategies using the patchwork phase-amplitude reduction because the dynamics are inherently discontinuous. Problems along these lines will be examined in future work.

6 Discussion and Conclusions

In this work, a general strategy is developed for calculating a phase-amplitude reduction of the form (9) for limit cycle oscillators that is valid to arbitrary orders accuracy in the amplitude coordinates. As part of this reduction strategy, the standard definition of asymptotic phase determined by the

isochrons (2) is used to characterize the timing of oscillations. Isostable coordinates [26] are used to characterize the transient decay in directions transverse to the periodic orbit. The key feature of both phase and isostable coordinates that allows for the high-accuracy reduction illustrated here is that they have simple dynamics in the absence of external perturbations in the entire basin of attraction of the limit cycle: the phase coordinate increases at a constant rate (i.e., $\dot{\theta} = \omega$) and the isostable coordinates decay exponentially (i.e., $\dot{\psi}_j = \kappa_j \psi_j$). This essential characteristic allows for the derivation of equations of the form (18), (34), and (44) that are used to compute the terms of the asymptotic expansions in the phase-amplitude reduction (9).

Examples given in this work compute the phase-amplitude reduced equations for the nonradial isochron clock (74) and a simplified model of circadian oscillations (75) to fourteenth order and eighth order, respectively, in the non-negligible isostable coordinates. To determine the appropriate equations of the form (18), (34), (44) that are used to compute the terms of the phase-amplitude reduction, the powers of the isostable coordinates in the expansions (30) and (40) must be matched. Additionally, powers of the isostable coordinates in the right hand sides of (15) and (12) must be matched. The resulting equations are easily identified for the lowest order terms of the expansions (for example, (16), (17)), but for higher order terms it is imperative to perform this matching process using a symbolic computational package because the number of terms that must be considered grows rapidly with the order of the expansion considered. The examples considered in this work are relatively low-dimensional but the proposed reduction strategy can be readily implemented in dynamical systems with much higher dimension.

While the phase-amplitude reduction (9) can in principle be performed to arbitrary orders of accuracy, in the examples considered here diminishing returns are observed as the order of accuracy of the reduction increases. For example, in the results shown in Figure 3B, the decrease in error observed between the zeroth and second order reduction is much more substantial than the decrease in error observed between the eighth and fourteenth order reductions. Additional analysis that characterizes the error resulting from the truncating specific higher order terms would be useful. Likewise, quantitative estimates relating the order of accuracy of the reduction and the size of the regions for which the reductions accurately reflect the unreduced system behavior would be useful. These lines of inquiry will be left for future work.

In applications where the applied perturbations are particularly large, the patchwork phase-amplitude reduction strategy may be more appropriate. As illustrated in Section 4 the patchwork phase-amplitude reduction framework incorporates multiple high-accuracy phase-amplitude reductions and actively switches between nominal orbits so that the isostable coordinate and hence the distance from the nominal periodic orbit remains small. Other reduction strategies have used a similar notion of an extended phase space [13] which considers a hypersurface formed by a family of limit cycles for various choices of a given parameter. The use of an extended phase space as in [13] allows for a reduced model that is valid when the perturbation can be decomposed to a large amplitude but slowly-varying component and a remaining weak fluctuation. The patchwork phase-amplitude reduction in the current work differs substantially from [13] as it explicitly incorporates amplitude coordinates for each limit cycle considered and can be implemented using arbitrary perturbations. In the examples presented in this work, a third order accurate patchwork phase-amplitude reduction significantly outperforms an eighth-order accurate non-patchwork phase-amplitude reduction for particularly large magnitude inputs allowing for the implementation of a simple but effective control strategy (77) that can be implemented to reduce the time required for reentrainment after sudden shifts in the environmental time.

While the reduction (10) can be computed to arbitrary order accuracy in ψ_j for $j = 1, \ldots, N$, during implementation of the reduction strategy the state dynamics associated with rapidly decaying isostable coordinates are often truncated [5], [28], [29] without significantly influencing the

overall applicability of the reduction. This is done for the example from (75), resulting in a reduction (9) that implicitly assumes the dynamics are on a hypersurface on which the rapidly decaying and hence neglected isostable coordinates are zero. Understanding the magnitude of error that is incorporated when these isostable coordinates are truncated is a particularly important consideration that is left unaddressed in this manuscript. For the model (75) (and other examples in previous work) isostable coordinates are eliminated from the associated reduction if the Floquet multipliers are deemed to be 'close enough' to zero. For high-dimensional systems, it is often the case that a large majority of computed Floquet multipliers are close enough to zero that they are within the limits of precision for floating point arithmetic; as such the corresponding isostable coordinates can clearly be ignored. For isostable coordinates with corresponding Floquet multipliers that are small but not minuscule (e.g., $|\lambda_j| \sim 0.1$) truncation will lead to some errors in the reduction but it is not currently possible to quantify the magnitude of the resulting error. Analysis of this nature will be critical for the continued development of phase-amplitude reduction techniques using isostable coordinates and will be the subject of future work.

The proposed high-accuracy reduction frameworks are particularly useful in the study of systems with periodic orbits that have small magnitude Floquet exponents; these systems are typically difficult to handle with standard phase reduction methods because even relatively small inputs can drive the state far from the nominal periodic orbit. Such systems often emerge when considering population oscillations, i.e., limit cycles that represent the group dynamics of a coupled population of oscillators [60], [61], [62]. Additionally systems with slowly varying parameters that describe adaptation [63] or memory [64] typically result in slowly decaying amplitude components and would be good candidates for this method of analysis. The implementation and analysis of high-accuracy phase reduction methods have led to the discovery and characterization of surprising behaviors observed in perturbed limit cycle oscillators that go beyond the weakly perturbed limit [65], [31], [30], [42], [13]. The reduction frameworks presented here represent a powerful strategy that can be used to understand nontrivial synchronization and entrainment behaviors that emerge in response to strong perturbations.

This material is based upon work supported by the National Science Foundation grant CMMI-1933583.

Appendix A Orthogonality Relationships Between Terms of the Asymptotic Expansions

The requirements (47) and (48) can be used to derive orthogonality relationships between the first order terms of the asymptotic expansion (22). To illustrate this, consider (48) taken to first order accuracy in the isostable coordinates $\psi_1, \ldots, \psi_{N-1}$,

$$\kappa_n \psi_n = \left[I_n(\theta) + \sum_{k=1}^{N-1} \left[\psi_k I_n^k(\theta) \right] \right]^T \left[F(x^\gamma(\theta)) + \sum_{k=1}^{N-1} \left[\frac{dg^k}{dt} \psi_k + g^k(\theta) \kappa_k \psi_k \right] \right]. \tag{A1}$$

Considering all order zero terms in the isostable coordinates, one finds that $0 = I_n(\theta)^T F(x^\gamma(\theta)) = \frac{1}{\omega} I_n(\theta)^T \frac{\partial x^\gamma}{\partial \theta}$. Therefore

$$I_n(\theta)^T \frac{\partial x^\gamma}{\partial \theta} = 0, \text{ for all } n. \tag{A2}$$

Considering the order one terms in the isostable coordinates, by examining all terms that are proportional to ψ_n one finds

$$I_n^k(\theta)^T F(x^\gamma(\theta)) + I_n(\theta)^T \frac{dg^k}{dt} + \kappa_k I_n(\theta)^T g^k(\theta) = \begin{cases} \kappa_n, & \text{if } k = n, \\ 0, & \text{otherwise.} \end{cases} \tag{A3}$$

Toward simplifying (A3), one can use (16) to write

$$\begin{aligned} I_n(\theta)^T \frac{dg^k}{dt} &= I_n(\theta)^T (J - \kappa_k \mathrm{Id}) g^k(\theta) \\ &= g^k(\theta)^T (J^T - \kappa_k \mathrm{Id}) I_n(\theta) \\ &= -g^k(\theta)^T \frac{dI_n}{dt} + (\kappa_n - \kappa_k) g^k(\theta)^T I_n(\theta), \end{aligned} \tag{A4}$$

where the last line is obtained using (41). Continuing to simplify (A4), one can write $\frac{dI_n}{dt} = \frac{\partial I_n}{\partial x}\frac{dx}{dt} = H_{\psi_n,\theta} F(x^\gamma(\theta))$ where $H_{\psi_n,\theta}$ is the Hessian of ψ_n evaluated at $x^\gamma(\theta)$ so that

$$\begin{aligned} I_n(\theta)^T \frac{dg^k}{dt} &= -g^k(\theta)^T H_{\psi_n,\theta} F(x^\gamma(\theta)) + (\kappa_n - \kappa_k) g^k(\theta)^T I_n(\theta), \\ &= -I_n^k(\theta)^T F(x^\gamma(\theta)) + (\kappa_n - \kappa_k) g^k(\theta)^T I_n(\theta), \end{aligned} \tag{A5}$$

where the last line is obtained using the relation that $H_{\psi_n,\theta} g^k(\theta) = I_n^k(\theta)$ (cf. [29]) and taking the transpose noting that the Hessian is symmetric. Finally, substituting (A5) into (A3) yields

$$\kappa_n g^k(\theta)^T I_n(\theta) = \begin{cases} \kappa_n, & \text{if } k = n, \\ 0, & \text{otherwise,} \end{cases} \tag{A6}$$

and thus

$$g^k(\theta)^T I_n(\theta) = \begin{cases} 1, & \text{if } k = n, \\ 0, & \text{otherwise.} \end{cases} \tag{A7}$$

A similar argument starting with (47) instead of (48) can be followed to find

$$\begin{aligned} Z(\theta)^T \frac{\partial x^\gamma}{\partial \theta} &= 1, \\ g^k(\theta)^T Z(\theta) &= 0 \text{ for all } k. \end{aligned} \tag{A8}$$

Appendix B Appropriately Aligning Periodic Orbits in the Implementation of the Patchwork Reduction

While (65) predicts that the periodic orbits match at predictable isostable coordinates provided the orbits are close enough to each other, they must be temporally aligned in order to implement the patchwork reduction. This issue is illustrated in Figure B1 for two separate periodic orbits $x_{p_1}^\gamma(\theta)$ and $x_{p_2}^\gamma(\theta)$ obtained for two different choices of the parameter p from (57). As illustrated in Panel A, these two orbits are aligned so that their respective maximums occur at $\theta = \pi$. Numerically, it is possible to identify an isostable value at which orbits are nearby as shown in panel B, however, these orbits will not necessarily be aligned in phase as required by (73) to convert coordinates between orbits. Alignment can be accomplished by appropriately shifting the orbit $x_{p_2}^\gamma$ by some value $\theta_s(p_1, p_2)$ as illustrated in Panel C. After this shift, the periodic orbits themselves are not

temporally aligned, as illustrated in panel D. Nonetheless, they are aligned near the expected switching point allowing one to implement the patchwork phase-amplitude reduction. This process can be repeated for multiple orbits and the function $\theta_s(p_i, p_j)$ can be defined that characterizes how much $x^\gamma_{p_j}$ has been shifted relative to $x^\gamma_{p_i}$ when all orbits are properly aligned.

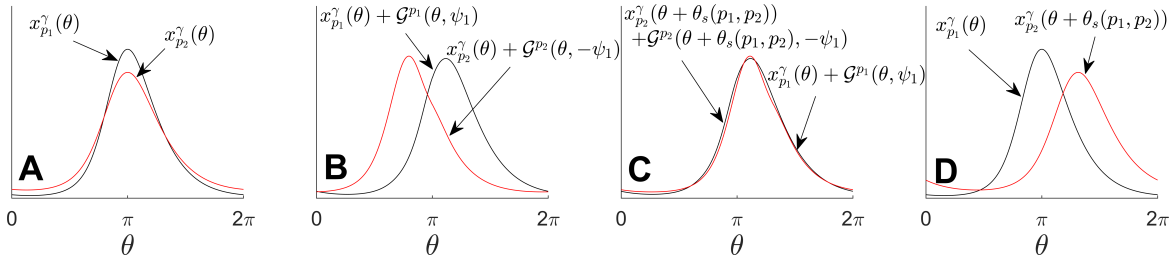

Figure B1: Panel A shows two orbits for two choices of parameters from (57) which are temporally aligned in the sense that their peaks occur at the same value of θ. Panel B illustrates that while these two orbits are close to each other for a given value of ψ_1, they are not temporally aligned. One can calculate $\theta_s(p_1, p_2)$ as in Panel C which shows the shift required to align the orbits from panel B. This shift is required in order to convert coordinates between orbits during the implementation of the patchwork phase-amplitude reduction because $\Delta\theta$ from (73) must remain small. Panel D emphasizes that after the orbits are aligned at the indicated isostable coordinates, the limit cycles themselves are no longer temporally aligned. This misalignment must be taken into account in the control strategy described by (77).

Appendix C Steps Required in the Computation of the High-Order Phase and Isostable Reduction

This appendix provides an overview of the practical steps required to compute the high-order phase-amplitude reduction (9) as detailed in Section 3. This is meant to aid an interested reader in implementing the reduction framework in a general model.

Step 1) For a given model, identify a target T-periodic orbit $x^\gamma(t)$. Choose some location on this periodic orbit to correspond to $\theta = 0$. Compute the fundamental matrix Φ and identify its eigenvalues λ_i and associated left eigenvectors w_j. Each nonunity eigenvalue corresponds to an isostable coordinate with Floquet exponent $\kappa_i = \log(\lambda_i)/T$. Isostable coordinates associated with eigenvalues of less than approximately 0.1 can be neglected from the reduction. Let $M \in \mathbb{N}$ denote the total number of isostable coordinates considered in the reduction.

Step 2) Use a symbolic computational package to take necessary derivatives and collect terms appropriately to write

$$\begin{bmatrix} \sum_{i=2}^{\infty} \frac{1}{i!} \left[\overset{i}{\otimes} \left[\sum_{k=1}^{M} \left[\psi_k g^k(\theta) \right] + \sum_{j=1}^{M} \sum_{k=1}^{j} \left[\psi_j \psi_k g^{jk}(\theta) \right] + \dots \right]^T \right] \operatorname{vec}(f_1^{(i)}(\theta)) \\ \vdots \\ \sum_{i=2}^{\infty} \frac{1}{i!} \left[\overset{i}{\otimes} \left[\sum_{k=1}^{M} \left[\psi_k g^k(\theta) \right] + \sum_{j=1}^{M} \sum_{k=1}^{j} \left[\psi_j \psi_k g^{jk}(\theta) \right] + \dots \right]^T \right] \operatorname{vec}(f_N^{(i)}(\theta)) \end{bmatrix}$$

$$= \sum_{j=1}^{M} \sum_{k=1}^{j} \left[\psi_j \psi_k q^{jk}(\theta) \right] + \sum_{i=1}^{M} \sum_{j=1}^{i} \sum_{k=1}^{j} \left[\psi_i \psi_j \psi_k q^{ijk}(\theta) \right] + \dots, \tag{C1}$$

where the terms $q^{ijk\cdots}(\theta)$ above match the periodic terms from equation (18). The terms on the left side of (C1) come from Equation (15). Save all resulting $q^{ijk\cdots}(\theta)$ functions so that they can be evaluated later.

Step 3) Compute each $g^{ijk\cdots}(\theta)$ by finding the necessary periodic orbits of equations of the form (18). These must be computed in ascending order, for instance, by computing all first order terms, followed by all second order terms, followed by third order terms and so on. For low dimensional systems, a Newton iteration can be used to identify the required periodic orbits. Normalize appropriately according to the comments from Section 3.1.1.

Step 4) Use a symbolic computational package to take necessary derivatives and collect terms appropriately to write

$$-\begin{bmatrix} a_1 & \cdots & a_N \end{bmatrix} \left(Z(\theta) + \sum_{k=1}^{M} \left[\psi_k Z^k(\theta) \right] + \sum_{j=1}^{M} \sum_{k=1}^{j} \left[\psi_j \psi_k Z^{jk}(\theta) \right] + \dots \right)$$

$$= \sum_{k=1}^{M} \left[\psi_k q_\theta^k(\theta) \right] + \sum_{j=1}^{M} \sum_{k=1}^{j} \left[\psi_j \psi_k q_\theta^{jk}(\theta) \right] + \sum_{i=1}^{M} \sum_{j=1}^{i} \sum_{k=1}^{j} \left[\psi_i \psi_j \psi_k q_\theta^{ijk}(\theta) \right] + \dots, \tag{C2}$$

and

$$-\begin{bmatrix} a_1 & \cdots & a_N \end{bmatrix} \left(I_n(\theta) + \sum_{k=1}^{M} \left[\psi_k I_n^k(\theta) \right] + \sum_{j=1}^{M} \sum_{k=1}^{j} \left[\psi_j \psi_k I_n^{jk}(\theta) \right] + \dots \right)$$

$$= \sum_{k=1}^{M} \left[\psi_k q_{\psi_n}^k(\theta) \right] + \sum_{j=1}^{M} \sum_{k=1}^{j} \left[\psi_j \psi_k q_{\psi_n}^{jk}(\theta) \right] + \sum_{i=1}^{M} \sum_{j=1}^{i} \sum_{k=1}^{j} \left[\psi_i \psi_j \psi_k q_{\psi_n}^{ijk}(\theta) \right] + \dots, \tag{C3}$$

where the terms $q_\theta^{ijk\cdots}(\theta)$ and $q_{\psi_n}^{ijk\cdots}(\theta)$ match those from (34) and (44), respectively. The terms on the left sides of (C2) and (C3) come from (30) and (40), respectively. Save all resulting $q_\theta^{ijk\cdots}(\theta)$ and $q_{\psi_n}^{ijk\cdots}(\theta)$ functions so that they can be evaluated later. Note that these functions will contain some $g^{ijk}(\theta)$ terms.

Step 5) Compute each $Z^{ijk\cdots}(\theta)$ and $I_n^{ijk\cdots}(\theta)$ by finding the necessary periodic orbits of equations of the form (34) and (44), respectively. These must also be computed in ascending order like the $g^{ijk\cdots}(\theta)$ functions. For numerical reasons, it is typically necessary to solve Equations (34) and (44) in backwards time. A Newton iteration can be used to identify the required periodic orbits. Normalize solutions (if necessary) so that (47) and (48) hold. Because the $Z^{ijk\cdots}(\theta)$ and $I_n^{ijk\cdots}(\theta)$ terms contain the $g^{ijk\cdots}(\theta)$ terms, Step 5 must be completed after Step 3.

References

[1] A. Winfree. *The Geometry of Biological Time*. Springer Verlag, New York, second edition, 2001.

[2] Y. Kuramoto. *Chemical Oscillations, Waves, and Turbulence*. Springer-Verlag, Berlin, 1984.

[3] G. B. Ermentrout and D. H. Terman. *Mathematical Foundations of Neuroscience*, volume 35. Springer, New York, 2010.

[4] A. Pikovsky, M. Rosenblum, and J. Kurths. *Synchronization: a universal concept in nonlinear sciences*. Cambridge University Press, Cambridge, 2001.

[5] B. Monga, D. Wilson, T. Matchen, and J. Moehlis. Phase reduction and phase-based optimal control for biological systems: a tutorial. *Biological Cybernetics*, 113(1-2):11–46, 2019.

[6] B. Pietras and A. Daffertshofer. Network dynamics of coupled oscillators and phase reduction techniques. *Physics Reports*, 2019.

[7] H. Nakao. Phase reduction approach to synchronisation of nonlinear oscillators. *Contemporary Physics*, 57(2):188–214, 2016.

[8] F. Dörfler, M. Chertkov, and F. Bullo. Synchronization in complex oscillator networks and smart grids. *Proceedings of the National Academy of Sciences*, 110(6):2005–2010, 2013.

[9] D. M. Abrams and S. H. Strogatz. Chimera states for coupled oscillators. *Physical Review Letters*, 93(17):174102, 2004.

[10] S. H. Strogatz, D. M. Abrams, A. McRobie, B. Eckhardt, and E. Ott. Theoretical mechanics: Crowd synchrony on the millennium bridge. *Nature*, 438(7064):43, 2005.

[11] A. V. Pimenova, D. S. Goldobin, M. Rosenblum, and A. Pikovsky. Interplay of coupling and common noise at the transition to synchrony in oscillator populations. *Scientific Reports*, 6:38518, 2016.

[12] K. Taira and H. Nakao. Phase-response analysis of synchronization for periodic flows. *Journal of Fluid Mechanics*, 846, 2018.

[13] W. Kurebayashi, S. Shirasaka, and H. Nakao. Phase reduction method for strongly perturbed limit cycle oscillators. *Physical Review Letters*, 111(21):214101, 2013.

[14] Y. Park and B. Ermentrout. Weakly coupled oscillators in a slowly varying world. *Journal of Computational Neuroscience*, 40(3):269–281, 2016.

[15] K. Pyragas and V. Novičenko. Phase reduction of a limit cycle oscillator perturbed by a strong amplitude-modulated high-frequency force. *Physical Review E*, 92(1):012910, 2015.

[16] H. M. Osinga and J. Moehlis. Continuation-based computation of global isochrons. *SIAM Journal on Applied Dynamical Systems*, 9(4):1201–1228, 2010.

[17] M. Detrixhe, M. Doubeck, J. Moehlis, and F. Gibou. A fast Eulerian approach for computation of global isochrons in high dimensions. *SIAM Journal on Applied Dynamical Systems*, 15(3):1501–1527, 2016.

[18] Y. Lan and I. Mezić. Linearization in the large of nonlinear systems and Koopman operator spectrum. *Physica D: Nonlinear Phenomena*, 242(1):42–53, 2013.

[19] B. Letson and J. E. Rubin. A new frame for an old (phase) portrait: Finding rivers and other flow features in the plane. *SIAM Journal on Applied Dynamical Systems*, 17(4):2414–2445, 2018.

[20] C. O. Diekman and A. Bose. Entrainment maps: a new tool for understanding properties of circadian oscillator models. *Journal of Biological Rhythms*, 31(6):598–616, 2016.

[21] D. Wilson and B. Ermentrout. An operational definition of phase characterizes the transient response of perturbed limit cycle oscillators. *SIAM Journal on Applied Dynamical Systems*, 17(4):2516–2543, 2018.

[22] J. Cui, C. C. Canavier, and R. J. Butera. Functional phase response curves: A method for understanding synchronization of adapting neurons. *Journal of Neurophysiology*, 102(1):387–398, 2009.

[23] P. C. Bressloff and J. N. MacLaurin. A variational method for analyzing stochastic limit cycle oscillators. *SIAM Journal on Applied Dynamical Systems*, 17(3):2205–2233, 2018.

[24] A. Mauroy, I. Mezić, and J. Moehlis. Isostables, isochrons, and Koopman spectrum for the action–angle representation of stable fixed point dynamics. *Physica D: Nonlinear Phenomena*, 261:19–30, 2013.

[25] D. Wilson and J. Moehlis. Isostable reduction of periodic orbits. *Physical Review E*, 94(5):052213, 2016.

[26] D. Wilson and B. Ermentrout. Greater accuracy and broadened applicability of phase reduction using isostable coordinates. *Journal of Mathematical Biology*, 76(1-2):37–66, 2018.

[27] S. Shirasaka, W. Kurebayashi, and H. Nakao. Phase-amplitude reduction of transient dynamics far from attractors for limit-cycling systems. *Chaos: An Interdisciplinary Journal of Nonlinear Science*, 27(2):023119, 2017.

[28] D. Wilson. Isostable reduction of oscillators with piecewise smooth dynamics and complex Floquet multipliers. *Physical Review E*, 99(2):022210, 2019.

[29] D. Wilson and B. Ermentrout. Augmented phase reduction of (not so) weakly perturbed coupled oscillators. *SIAM Review*, 61(2):277–315, 2019.

[30] Iván León and Diego Pazó. Phase reduction beyond the first order: The case of the mean-field complex Ginzburg-Landau equation. *Physical Review E*, 100(1):012211, 2019.

[31] M. Rosenblum and A. Pikovsky. Numerical phase reduction beyond the first order approximation. *Chaos: An Interdisciplinary Journal of Nonlinear Science*, 29(1):011105, 2019.

[32] J. Guckenheimer. Isochrons and phaseless sets. *Journal of Mathematical Biology*, 1(3):259–273, 1975.

[33] K. C. A. Wedgwood, K. K. Lin, R. Thul, and S. Coombes. Phase-amplitude descriptions of neural oscillator models. *The Journal of Mathematical Neuroscience*, 3(1):2, 2013.

[34] B. Letson and J. E. Rubin. LOR for analysis of periodic dynamics: A one-stop shop approach. *SIAM Journal on Applied Dynamical Systems*, 19(1):58–84, 2020.

[35] A. Guillamon and G. Huguet. A computational and geometric approach to phase resetting curves and surfaces. *SIAM Journal on Applied Dynamical Systems*, 8(3):1005–1042, 2009.

[36] D. Jordan and P. Smith. *Nonlinear Ordinary Differential Equations: An Introduction for Scientists and Engineers*, volume 10. Oxford University Press, Oxford, 2007.

[37] M. D. Kvalheim and S. Revzen. Existence and uniqueness of global Koopman eigenfunctions for stable fixed points and periodic orbits. *arXiv preprint arXiv:1911.11996*, 2019.

[38] I. Mezić. Spectrum of the Koopman operator, spectral expansions in functional spaces, and state-space geometry. *Journal of Nonlinear Science*, pages 1–55, 2019.

[39] A. Mauroy and I. Mezić. Global computation of phase-amplitude reduction for limit-cycle dynamics. *Chaos: An Interdisciplinary Journal of Nonlinear Science*, 28(7):073108, 2018.

[40] E. Brown, J. Moehlis, and P. Holmes. On the phase reduction and response dynamics of neural oscillator populations. *Neural Computation*, 16(4):673–715, 2004.

[41] O. Castejón, A. Guillamon, and G. Huguet. Phase-amplitude response functions for transient-state stimuli. *J. Math. Neurosci*, 3:13, 2013.

[42] D. Wilson and B. Ermentrout. Phase models beyond weak coupling. *Physical Review Letters*, 123(16):164101, 2019.

[43] D. Takeshita and R. Feres. Higher order approximation of isochrons. *Nonlinearity*, 23(6):1303, 2010.

[44] O. Suvak and A. Demir. Quadratic approximations for the isochrons of oscillators: a general theory, advanced numerical methods, and accurate phase computations. *IEEE Transactions on Computer-Aided Design of Integrated Circuits and Systems*, 29(8):1215–1228, 2010.

[45] J. R. Magnus and H. Neudecker. *Matrix differential calculus with applications in statistics and econometrics*. John Wiley & Sons, Chistester, 2007.

[46] W. W. Hager. Updating the inverse of a matrix. *SIAM Review*, 31(2):221–239, 1989.

[47] J. A. Sanders, F. Verhulst, and J. Murdock. *Averaging Methods in Nonlinear Dynamical Systems*. Springer-Verlag, New York, second edition, 2007.

[48] J. Guckenheimer and P. Holmes. *Nonlinear Oscillations, Dynamical Systems, and Bifurcations of Vector Fields*, volume 42. Springer Verlag, New York, 1983.

[49] C. H. Johnson, J. A. Elliott, and R. Foster. Entrainment of circadian programs. *Chronobiology International*, 20(5):741–774, 2003.

[50] C. A. Czeisler, J. F. Duffy, T. L. Shanahan, E. N. Brown, J. F. Mitchell, D. W. Rimmer, J. M. Ronda, E. J. Silva, J. S. Allan, J. S. Emens, D. J. Dijk, and R. E. Kronauer. Stability, precision, and near-24-hour period of the human circadian pacemaker. *Science*, 284(5423):2177–2181, 1999.

[51] K. P. Wright, R. J. Hughes, R. E. Kronauer, D. J. Dijk, and C. A. Czeisler. Intrinsic near-24-h pacemaker period determines limits of circadian entrainment to a weak synchronizer in humans. *Proceedings of the National Academy of Sciences*, 98(24):14027–14032, 2001.

[52] J. Arendt. Managing jet lag: some of the problems and possible new solutions. *Sleep Medicine Reviews*, 13(4):249–256, 2009.

[53] R. L. Sack. Jet lag. *New England Journal of Medicine*, 362(5):440–447, 2010.

[54] J. C. Leloup and A. Goldbeter. Critical phase shifts slow down circadian clock recovery: implications for jet lag. *Journal of Theoretical Biology*, 333:47–57, 2013.

[55] Z. Lu, K. Klein-Cardeña, S. Lee, T. M. Antonsen, M. Girvan, and E. Ott. Resynchronization of circadian oscillators and the east-west asymmetry of jet-lag. *Chaos: An Interdisciplinary Journal of Nonlinear Science*, 26(9):094811, 2016.

[56] N. Bagheri, J. Stelling, and F. J. Doyle III. Circadian phase resetting via single and multiple control targets. *PLoS Computational Biology*, 4(7):e1000104, 2008.

[57] D. A. Dean, D. B. Forger, and E. B. Klerman. Taking the lag out of jet lag through model-based schedule design. *PLoS Computational Biology*, 5(6):e1000418, 2009.

[58] K. Serkh and D. B. Forger. Optimal schedules of light exposure for rapidly correcting circadian misalignment. *PLoS Computational Biology*, 10(4):e1003523, 2014.

[59] D. Gonze, S. Bernard, C. Waltermann, A. Kramer, and H. Herzel. Spontaneous synchronization of coupled circadian oscillators. *Biophysical Journal*, 89(1):120–129, 2005.

[60] Y. Kawamura, H. Nakao, K. Arai, H. Kori, and Y. Kuramoto. Collective phase sensitivity. *Physical Review Letters*, 101(2):024101, 2008.

[61] K. Kotani, I. Yamaguchi, L. Yoshida, Y. Jimbo, and G. B. Ermentrout. Population dynamics of the modified theta model: macroscopic phase reduction and bifurcation analysis link microscopic neuronal interactions to macroscopic gamma oscillation. *Journal of The Royal Society Interface*, 11(95):20140058, 2014.

[62] Z. Levnajić and A. Pikovsky. Phase resetting of collective rhythm in ensembles of oscillators. *Physical Review E*, 82(5):056202, 2010.

[63] Bard Ermentrout. Linearization of FI curves by adaptation. *Neural computation*, 10(7):1721–1729, 1998.

[64] E. M. Cherry and S. J. Evans. Properties of two human atrial cell models in tissue: restitution, memory, propagation, and reentry. *Journal of Theoretical Biology*, 254(3):674–690, 2008.

[65] D. S. Goldobin, J. Teramae, H. Nakao, and G. B. Ermentrout. Dynamics of limit-cycle oscillators subject to general noise. *Physical Review Letters*, 105(15):154101, 2010.